**Title:** Deficits in Behavioral and Neuronal Pattern Separation in Temporal Lobe Epilepsy

**Abbreviated Title**: Pattern Separation and Mnemonic Discrimination in Epilepsy

**Authors and Affiliations**: A.D. Madar[1,2], J.A. Pfammatter[1], J. Bordenave[3], E.I. Plumley[3], S. Ravi[1], M. Cowie[1], E.P. Wallace[1,3], B.P. Hermann[3], R.K. Maganti[3], M.V. Jones[1]

[1]Department of Neuroscience, University of Wisconsin-Madison, 53703

[2]Department of Neurobiology, Grossman Institute for Neuroscience, Quantitative Biology and Human Behavior, University of Chicago, 60637

[3]Department of Neurology, University of Wisconsin-Madison, School of Medicine and Public Health

**Acknowledgement:** We thank Lin Lin who helped start behavioral tests in mice in the Jones lab and Drs. C.E.L Stark and M.A. Yassa for allowing us to use software and materials they developed.

**Author contributions:** Conceptualization: MVJ, ADM. Data curation: ADM, JAP. Formal analysis: ADM, JAP, MVJ. Funding acquisition: MVJ, ADM, RKM, JAP. Investigation: ADM, JAP, JB, EIP, SR, MC, EPW. Methodology: ADM, JAP, MVJ. Project administration: JAP, ADM, MVJ. Resources: MVJ, BPH, RKM. Software: ADM, JAP, MVJ. Supervision: MVJ. Validation: JAP, ADM. Visualization: ADM, JAP, MVJ. Writing – original draft: ADM. Writing – review & editing: all authors

**Funding:** This work was supported by the US National Institutes of Health (MVJ: RO1 NS075366), the University of Wisconsin Institute for Clinical and Translational Research (MVJ.; NIH/NCATS UL1TR000427), the US Department of Defense (RKM: PR161864) and Lily's Fund for Epilepsy Research (ADM.; 2015 fellow).

**Conflicts of Interest:** The authors declare no conflict of interest.

**Abstract:**

In temporal lobe epilepsy, the ability of the dentate gyrus to limit excitatory cortical input to the hippocampus breaks down, leading to seizures. The dentate gyrus is also thought to help discriminate between similar memories by performing pattern separation, but whether epilepsy leads to a breakdown in this neural computation, and thus to mnemonic discrimination impairments, remains unknown. Here we show that temporal lobe epilepsy is characterized by behavioral deficits in mnemonic discrimination tasks, in both humans and mice. Using a recently developed assay in brain slices of the same epileptic mice, we reveal a decreased ability of the dentate gyrus to perform certain forms of pattern separation. This is due to a subset of granule cells with abnormal bursting that can develop independently of early EEG abnormalities. Overall, our results linking physiology, computation and cognition in the same mice, advance our understanding of episodic memory mechanisms and their dysfunction in epilepsy.

**Keywords**:

Patch-clamp, low-dose systemic kainate model**,** kainic acid, interictal spikes, novelty recognition, firing rate, spiking patterns, similarity metrics, input-output, entorhinal cortex, perforant path, EPSC, excitation/inhibition ratio, dentate gate, Hebb-Marr theory

## Introduction:

Temporal lobe epilepsy (TLE) represents about 60% of all epilepsy cases, a third of which are refractory to medication (Tellez-Zenteno and Hernandez-Ronquillo, 2012). TLE is characterized by recurring focal seizures originating in or near the hippocampus (Toyoda et al., 2013), microcircuit pathologies in brain regions including the hippocampus (Alexander et al., 2016) and memory-related cognitive deficits (Helmstaedter et al., 2003; Zhao et al., 2014). Although the hippocampus is a nexus for episodic memory that is critically affected during TLE, the relationship between TLE and hippocampus-dependent memory is insufficiently understood.

Episodic memory formation is thought to involve storage of neural representations in area CA3 of the hippocampus via Hebbian plasticity at recurrent excitatory synapses of coactivated cells (Rolls, 2010). In this view, a partial cue reactivates a subset of the CA3 ensemble that in turn recruits the other neurons of the original pattern resulting in recall of the original event (Rolls, 2010). However, recurrent excitation is problematic because it theoretically a) predisposes the network to over-excitation that could trigger seizures (Le Duigou et al., 2014) and b) limits the number of patterns that can be stored without overlap (Rolls, 2010). Overlapping memory representations would in turn lead to interference during recall and thus cognitive confusion. To solve these problems, it was proposed that the dentate gyrus (DG) of the hippocampus acts as a) a gate and b) a pattern separator, so that similar cortical representations are transformed into sparse and dissimilar patterns before reaching CA3 (O'Reilly and McClelland, 1994; Hsu, 2007; Treves et al., 2008; Dengler and Coulter, 2016).

The function of DG as a gate for cortical activity to prevent seizure generation fails in TLE (Hsu, 2007; Krook-Magnuson et al., 2015; Dengler and Coulter, 2016; Lu et al., 2016): granule cells (GCs), the output neurons of DG, lose their usual sparseness due to network

reorganization (Artinian et al., 2011; Dengler and Coulter, 2016; Dengler et al., 2017) making cortical excitation easier to propagate to CA3 (Behr et al., 1998; Patrylo et al., 1999; Ouedraogo et al., 2016). Even in healthy animals, repeated excitation of GCs induces seizures (Krook-Magnuson et al., 2015) and prolonged stimulation of DG causes TLE (Sloviter, 1983).

An alternate view of the DG function, developed in parallel to the concept of dentate gate, is that it performs pattern separation: the transformation of similar cortical patterns into dissimilar hippocampal representations. This process theoretically supports mnemonic discrimination, the ability to distinguish between similar memories. Indeed, DG lesions impair mnemonic discrimination both in rodents (Treves et al., 2008; Kesner and Rolls, 2015; Kesner et al., 2016) and humans (Yassa et al., 2011; Baker et al., 2016; Bennett and Stark, 2016; Dillon et al., 2017). Moreover, computational models (Chavlis and Poirazi, 2017) and recent experiments (Knierim and Neunuebel, 2016; Berron et al., 2016; Madar et al., 2019a, b) suggest that the DG circuitry supports multiple forms of pattern separation (Santoro, 2013). Whether such computations underlie mnemonic discrimination remains unknown.

Unsurprisingly, TLE negatively impacts hippocampal-dependent memory in humans (Coras et al., 2014) and rodents (Groticke et al., 2008; Muller et al., 2009; Inostroza et al., 2013; Lenck-Santini and Scott, 2015). However, the effect of TLE specifically on DG computations and DG-dependent cognition remains understudied. It was only recently reported that patients with TLE are impaired at spatial mnemonic discrimination (Reyes et al., 2018) and that TLE causes deficits in DG-dependent object location memory in mice (Bui et al., 2018). A computational model has also suggested that hippocampal pathologies in TLE would degrade DG pattern separation (Yim et al., 2014) but the hypotheses that 1) TLE causes a breakdown in

DG neural pattern separation and 2) that such a failure causes mnemonic discrimination impairments remain experimentally untested.

Here we tested, in humans and mice, whether TLE is characterized by deficits in mnemonic discrimination and then recorded, in brain slices from the same mice, the spiking patterns of single GCs in response to parametrically varied afferent stimulation in order to gauge neuronal pattern separation.

## Materials and Methods:

***Human Behavior.*** A mnemonic similarity task (Stark et al., 2019), also known as a behavioral pattern separation (BPS) task (Stark et al., 2013), was administered to 15 patients in the University of Wisconsin-Madison Epilepsy Monitoring Unit. Under an approved Institutional Review Board protocol and after obtaining informed consent, the task was administered in conjunction with a standard neuropsychiatric evaluation and during electroencephalographic (EEG) recording, both of which are part of standard practice for diagnosing the patients' seizures. Patients were 18-65 years old, male and female. Only patients with a preliminary diagnosis of TLE were included in our analysis. As controls, 20 subjects without epilepsy, recruited to match the patients' age and sex distributions (family members of the patients when possible, or other volunteers), were also tested. Consent documents, medical records and primary data are on file in a secure location within the Dept. of Neurology. Data were deidentified prior to analysis. Subjects received no compensation for participation.

The visual, object recognition-based BPS task is described in Yassa et al. (2011) and has been further validated by demonstrating mnemonic discrimination deficits during normal aging and multiple neurologic and psychiatric disorders (Stark et al., 2019). It was implemented on a

laptop by trained neuropsychiatric postdoctoral fellows (J.B. and E.I.P.) using software distributed freely by the Stark lab (http://faculty.sites.uci.edu/starklab/mnemonic-similarity-task-mst/). Briefly, participants viewed a series of pictures of everyday objects (**Figure 1A**). During Phase 1, 128 different images were presented and the subject was asked to classify each as "indoor" or "outdoor", simply to engage the subject's attention. During Phase 2, a new series of 192 images was presented: 1/3 repeated from Phase 1 (*Repeated*), 1/3 new but similar to images from Phase 1 (*Lure*), and 1/3 new and completely different from Phase 1 (*Novel*). Participants were asked to classify each image of the Phase 2 set as "Old", "Similar", or "New". BPS was evaluated with a *discrimination index* computed as the difference between p("Similar"|Lure) and p("Similar"|Novel), as in past research (Yassa et al., 2011; Stark et al., 2019).

***Mouse Experiments.*** Male mice (C57BL6J, 5-6 weeks old) were received from Envigo (formerly Harlan, Madison, WI), housed in groups and allowed to acclimate to their new home environment for one or two weeks. Animals then underwent epilepsy induction with kainic acid (KA) injections (see below) (J.A.P.). A control group of mice was injected with saline and another received no injection: both were pooled together and considered as the control group because our analyses did not reveal any difference. 7-9 weeks after injection, mice started 4 weeks of behavioral testing on the BPS task. After completion of behavioral testing, animals (~18-20 weeks old) were transferred to a different building for EEG implantation. Each animal was recorded continuously for three days before being transferred back to the original building and sacrificed for slice electrophysiology (~20-24 weeks old). After each building-to-building transfer, mice were allowed a period of acclimation ranging from two days to two weeks. Behavioral testing (J.A.P, S.R. and M.C.), EEG recordings (E.P.W.) and slice electrophysiology

(A.D.M) were performed by different researchers, all of whom were blind to KA or Control treatments.

***Epilepsy induction.*** During the induction process, when not being handled, mice were individually housed in enclosed ~150 $cm^3$ acrylic cubicles with opaque sides and clear front portals with holes to allow air exchange, food and bedding. Animals were then randomly assigned to KA or Control treatment, ear punched for identification and weighed. Animals were induced for epileptogenesis using the repeated low-dose kainate method (Hellier et al., 1998; Sharma et al., 2018): a series of intraperitoneal injections based on the following schedule. Animals first received 10 mg/kg of kainic acid (Tocris Bioscience, UK) mixed in 1x PBS (8 ml per 10 mg) prepared from PBS tablets (Dot Scientific, Michigan) with deionized distilled water and filter sterilized (Millipore, Burlington, MA). Control animals were injected with an equivalent volume of saline made of 1x PBS. Animals continued to receive injections at 5mg/kg every 20 minutes until status epilepticus (SE) occurred (same number of saline injections in control mice). Some animals received alternating 5mg/kg and 2.5 mg/kg injections after the initial 10 mg/kg dose, but we found this schedule took more time than 5 mg/kg injections and our survival rate (>90% across all cohorts) was no different between the two schedules. Animals were considered to be in SE when displaying persistent behavioral seizures of level 4-5 on the Racine Scale (Racine, 1972), less than 5 minutes apart, for a minimum of 30 minutes. Animals received 4-9 injections depending on tolerance to kainic acid and injection schedule. After the injection schedule, animals were given fresh apple slices, monitored until SE ceased (assessed from normal posturing, within 1-1.5 hours), and returned to group housing. They were monitored, weighed and animals weighing less than their preinjection levels were given 0.4 ml of 1x PBS via intraperitoneal injection on a daily basis until their weight exceeded preinjection

level. No animal injected with saline ever experienced status epilepticus, lost weight, or required recovery injections of 1x PBS. Mice remained in the vivarium for 7-9 weeks after injections, allowing time for the development of epilepsy in KA mice (the latent period in the KA model of TLE has previously been evaluated as 10-30 days before the first spontaneous electrographic seizure, and ~11±5.4 weeks before the first spontaneous convulsive seizure (Levesque and Avoli, 2013). During this time some KA mice became aggressive and many of the aggressor animals were removed from group housing and caged individually.

***Mouse Behavior.*** At 14-16 weeks of age, mice started behavioral testing on a variant of a novelty recognition-based BPS task that is well established in rodents to report mnemonic discrimination abilities (van Hagen et al., 2015). Our protocol lasted 4 weeks, including 1 week of habituation and 3 weeks of trials. During the first week of habituation, each mouse was gently handled by the experimenter for five minutes every day. On the second week mice were split into three groups (A, B, and C). Each group went through a three-day schedule where animals were habituated on the first and second days and performed the object location task on the third day. Groups were staggered by one day each, such that group A was scheduled Monday-Wednesday, B Tuesday-Thursday and C Wednesday-Friday. Animals were housed following a 12:12 light-dark cycle and always handled or tested between 1 pm and 4pm (light period).

The arena used for the BPS task (see **Figure 3A**) was a 63.5 x 63.5 x 15 cm open topped Plexiglas box wrapped on the outside and bottom with black felt cloth. On each side of the arena were different images serving as proximal cues for orientation. The room also had numerous distinct distal cues (e.g. the video camera placed over the center of the arena, shelving, etc.), that were kept unchanged. During behavioral testing, the room was lit with a single bank of overhead fluorescent lamps.

For the BPS task, animals underwent three phases of exploration in the arena, each lasting 3 min and separated by 1.5 min of single housing in a solitary chamber. In Phase 1 (habituation) the arena was empty, in Phase 2 (sampling) the arena contained two identical objects in the center, and in Phase 3 (testing) one object had been randomly selected and displaced by a distance of 7, 14 or 21 cm. The arena and objects were cleaned with 70% ethanol before and after each phase. During Phases 2 and 3, the experimenter recorded the amount of time that the mouse spent interacting with each object with two silent stopwatches. The mouse was considered to be interacting with an object if it was within 1 cm of it and oriented towards, sniffing, scratching, or on top of the object. These three phases were repeated three times with a different distance each week, with the order of distances randomized. Objects used for the task were ~6 cm tall block style plastic colored figures or metal cylinders, with a footprint of ~2 cm in diameter.

All phases of the experiment were recorded with a 1080p webcam positioned above the arena. During all phases, the experimenter sat in the corner of the room out of the line of sight of the mouse. The experimenter was consistent in appearance and smell (e.g., same experimenter for a given cohort, wearing same white lab coat and gloves of the same color each day; use of scented soap, etc. was minimized).

***BPS Analysis.*** The discrimination ratio for each trial was computed as $(T_{moved} - T_{unmoved}) / T_{total}$ where $T_{moved}$ is the time spent exploring the moved object, $T_{unmoved}$ is the time spent exploring the unmoved object and $T_{total}$ is the sum of $T_{moved}$ and $T_{unmoved}$. The exploration times used to calculate the reported discrimination ratio were manually collected by experimenters during the BPS task. We (M.V.J. and J.A.P.) also developed a home-written program using video recordings for motion-tracking and trajectory analysis of each mouse during behavioral testing.

Discrimination ratios computed from automated tracking data were well correlated to the ratios from manually recorded times, and led to similar results ($R^2$ = 0.68, T(117) = 16.07, P < 0.001). Automated tracking data were also used to assess a) distance traveled as an estimate of motility and exploration and b) tendency to stay close to walls (i.e., thigmotaxis) as an estimate of anxiety. Thigmotaxis (Simon et al., 1994) was evaluated as the proportion of time spent within 6.35 mm of the wall (10% of the arena width).

***Mouse electroencephalography (EEG).*** EEG electrode implantation was performed at ~18-20 weeks of age for all animals, following a previously established protocol (Wallace et al., 2015). Briefly, mice were anesthetized with isoflurane and stainless steel screw electrodes were implanted in the skull (bregma +1.5 mm and 1 mm right, bregma -3 mm and 1 mm left, and lamda -1 mm at midline). Two stainless steel braided wires were placed in the nuchal muscles for electromyography (EMG) recording. After a 72 hour recovery, we transferred mice into individual tethered EEG acquisition chambers and allowed a >12 hour acclimation period. We acquired EEG and EMG signals continuously for 3 days. Recordings were digitized with an XLTek amplifier (XLTEK, USA) sampled at 1024 Hz. Ad libitum access to food and water was ensured.

***Interictal spike (IIS) analysis.*** In humans and most animal models of acquired TLE, overt seizures are relatively rare (often much less than once per day) (Levesque et al., 2016). In contrast, nonconvulsive and subclinical epileptiform events such as interictal spikes (IISs) can be very frequent, as much as many hundreds per day. Therefore, in order to assess epileptiform activity in KA animals, we used a modification of our previously published principal components (PC)-based method to quantify IISs (Pfammatter et al., 2018) and calculated an "Hourly IIS index" for each animal. All detected high-amplitude EEG events from 9 Ctrl and 15

KA animals were projected into the space spanned by their first three PCs. The main modification here is that, instead of using a Gaussian Mixture Model (GMM) to assign events to 'clusters', we simply gridded the PC space into 'voxels' and computed relevant quantities within each voxel exactly as we computed those same quantities within GMM 'clusters' previously: 1) The probability that events within a voxel are characteristic of an epileptogenic treatment (i.e., KA) was computed as the voxel-wise proportion of events coming from KA mice, 2) Only the voxels above chance level were considered specific to epileptogenic treatment and probabilities were scaled accordingly, 3) The Hourly IIS Index of a given animal was defined as the average frequency of detected events weighted by the scaled probabilities of each event's voxel. This new voxel-based method has the advantages to make no assumptions about the structure of the data in PC space or about the number of clusters to fit. Instead, the main free parameter is now the voxel volume: we selected a size of 10 cubic PC units following the same optimization procedure described in Pfammatter et al. (2018) in order to avoid overfitting. Extensive exploration (not shown) revealed that the final results are similar to the GMM method and are not importantly affected by moderate changes in voxel volume.

***Slice electrophysiology.*** Mice used for electrophysiology were p115-p182 at the time of experiment (mean ± SEM: p141 +/- 4 days; no difference in age between treatments: KA n = 13, Ctrl n = 6, U-test: P = 0.9, Z = 0.2, rank sum = 246). Age was also not correlated with any summary statistics presented in this study.

Adult mice were euthanized by transcardial perfusion with oxygenated PBS under isoflurane anesthesia, before decapitation and brain extraction. 400 μm horizontal slices of the ventral and intermediate hippocampus were prepared as detailed in Madar et al. (2019a). After slicing in a sucrose-based cutting solution (Yi et al., 2015), slices were transferred to an

incubation chamber filled with 50% cutting solution and 50% artificial cerebrospinal fluid (aCSF) at 37°C for 30 minutes, then room temperature. Patch-clamp recordings were done in a chamber submerged with aCSF containing (in mM) 125 NaCl, 25 NaHCO3, 2.5 KCl, 1.25 NaH2PO4, 2 CaCl2, 1 MgCl2, and 25 D-Glucose, flowing at 5 ml/min and saturated with a gas mixture of 95% $O_2$ and 5% $CO_2$. Stimulation was applied through a double-barreled "theta" pipette filled with aCSF. Patch pipettes were filled with an intracellular solution of the following composition (in mM): 135 K-gluconate, 5 KCl, 0.1 EGTA, 10 HEPES, 20 Na-Phosphocreatine, 2 $Mg_2$-ATP, 0.3 Na-GTP, 0.25 $CaCl_2$ adjusted to pH 7.3 with KOH and 310 mOsm with $H_2O$, leading to a 2-5 MΩ pipette resistance in aCSF. Whole-cell patch-clamp recordings of single DG GCs in response to electric stimulation of the outer molecular layer (perforant path) were performed as detailed in Madar et al. (2019a) (see **Figure 4A**), and the stimulation protocols used to test neural pattern separation were the same as in Madar et al.(2019b) (see **Figure 4B** and **5**). Briefly, input sets used for stimulation were composed of five (type 1) or ten (type 2 and 3) spiketrains (two seconds long), delivered sequentially (separated by five seconds of pause) and repeated ten or five times, respectively, in order to yield fifty output spiketrains. The stimulation pipette was placed >100µm lateral to the recorded GC to avoid direct stimulation of GC dendrites, with the baseline membrane potential held at -70 mV for current and voltage-clamp recordings (see **Figure 4A-B, 7B**).

Intrinsic electrophysiological properties of recorded GCs were the following (mean ± SEM for Ctrl / KA): resting membrane potential $V_{rest}$ = -78.0 ± 1.9 / -81.4 ± 1.2 mV; membrane resistance $R_m$ = 139 ± 17 / 178 ± 16 MΩ; membrane capacitance $C_m$ = 18 ± 1.2 / 17 ± 0.7 pF. There were no significant differences between control and KA mice (U-tests: P = 0.1, 0.2, 0.7; Z = 1.6, -1.2, 0.4; rank sums = 294, 198.5, 252.5 respectively).

***Neural pattern separation analysis.*** Similarity between spiketrains was assessed as in Madar et al. (2019a, b), using three metrics based on dividing spiketrains into time bins of a specific duration $\tau_w$: the Pearson's correlation coefficient (R), the normalized dot product (NDP) and the scaling factor (SF). NDP and SF consider spiketrains as vectors of spike count per bin and measure the angle (NDP is the cosine) and the ratio of norms (SF) between the two vectors. R considers vectors of deviation from mean spike count, which loses the original angle between the vectors of raw spike counts and leads to considering common periods of silence as correlated, unlike NDP. Both R and NDP are sensitive to binwise synchrony, whereas SF is more sensitive to differences in firing rate and burstiness (see Madar et al. 2019b for a detailed discussion on the different neural codes assumed by each metric). To further test the role of various spiketrain features in mediating pattern separation, we also considered neural codes purely focused on either 1) the average firing rate (FR), 2) the compactness (1 - proportion of time bins with at least one spike) and 3) the occupancy (average number of spikes in bins with at least one spike). These were computed as in Madar et al. (2019b) and the degree of pattern separation (or convergence, for negative values) was evaluated as the difference between the dispersion of the output spiketrains minus the dispersion of the input spiketrains. The dispersion was computed as the mean absolute value of pairwise differences for each spiketrain feature (FR, Compactness or Occupancy) over all spiketrains of a set, excluding self-comparisons and, in the case of the output sets, all comparisons between output spiketrains resulting from the same input spiketrain. When using a similarity metric S (R, NDP or SF), pattern separation was assessed following the same logic. First, the similarity between each pair of spiketrains of a given set was computed. $S_{input}$ was the average for all pairs of an input set (excluding self-comparisons), and $S_{output}$ was the average of all pairs in output sets excluding comparisons between output spiketrains coming

from repetitions of the same input train. This yielded a single output similarity value for a given output set, and the degree of pattern separation was thus $S_{input}$ - $S_{output}$. To gain a finer view, we also performed a pairwise analysis (as in Madar et al. 2019b) where each of the pairwise $S_{input}$ of an input set were distinguished (10 pairs for input sets of type 1, 45 pairs for input sets of type 2 and 3). The pairwise $S_{output}$ (pw $S_{output}$) was thus the average similarity across all pairs of output spiketrains resulting from a given pair of input spiketrains. Pattern separation was computed as pw $S_{input}$ – pw $S_{output}$.

***Software and statistics.*** Data analysis was performed using MATLAB (Mathworks, Natick, MA, USA). The Lilliefors test was used to verify the normality of data distributions (Lilliefors, 1967). Parametric or nonparametric statistical tests were appropriately used to assess significance (p-value < 0.05). Throughout the Results section, KW ANOVA corresponds to the nonparametric Kruskal-Wallis analysis of variance, U-test corresponds to the Wilcoxon rank-sum test equivalent to the Mann-Whitney U-test, and KS test corresponds to the two-sample Kolmogorov-Smirnov test (sidedness is specified in the legends).

To analyze performance of mice on the BPS task (**Figure 3B**) we performed a two-way ANOVA with the Matlab function *anova* based on a linear mixed-effects model built using *fitlme*, with the distance of the moved object as a continuous fixed effect, animal treatment (Ctrl vs. KA) as a categorical fixed effect, and animal identity nested within object distances as a random effect to account for repeated measurements. The same procedure was used for each panel in **Figure 3D-E.**

To determine whether ($S_{input}$, $S_{output}$) distributions were significantly different (**Figures 4-5**), we performed an analysis of the covariance (ANCOVA) using separate parabolic or linear

regression models, implemented in MATLAB with a custom-written code following the method described in (Motulsky and Ransnas, 1987), as in Madar et al. (2019a, b)

In **Figure 8A**, the non-linear regression was performed using the Matlab function *fitnlm* with a three-parameter model function $f(x) = \ a/(x+b)+c$

**Results:**

***Behavioral pattern separation deficits in TLE.*** Mnemonic discrimination is often called behavioral pattern separation (BPS) because it is hypothesized to be the behavioral outcome of neural pattern separation. It is the ability to discriminate between similar experiences (event, environment, object, etc.) that occurred at different times (Santoro, 2013). Multiple BPS tasks have been demonstrated to be DG-dependent in humans (Baker et al., 2016) and rodents (Kesner and Rolls, 2015; Kesner et al., 2016; Bui et al., 2018). We thus chose some of these established tasks to test whether TLE impacts DG-dependent cognition, both in humans and mice.

In humans, we used the object recognition-based *Mnemonic Similarity Task* developed by the Stark lab (Stark et al., 2019), where participants must distinguish between similar images presented at different times (**Figure 1A**, **Materials and Methods – Human behavior**). Patients previously diagnosed with TLE showed a severe deficit (~50%) compared to nonepileptic subjects in their ability to correctly identify objects as being similar but not identical (**Figure 1**). These results confirmed our hypothesis that TLE impairs DG-dependent mnemonic discrimination, thus warranting further study of the impact of TLE on DG computations that might explain this cognitive deficit.

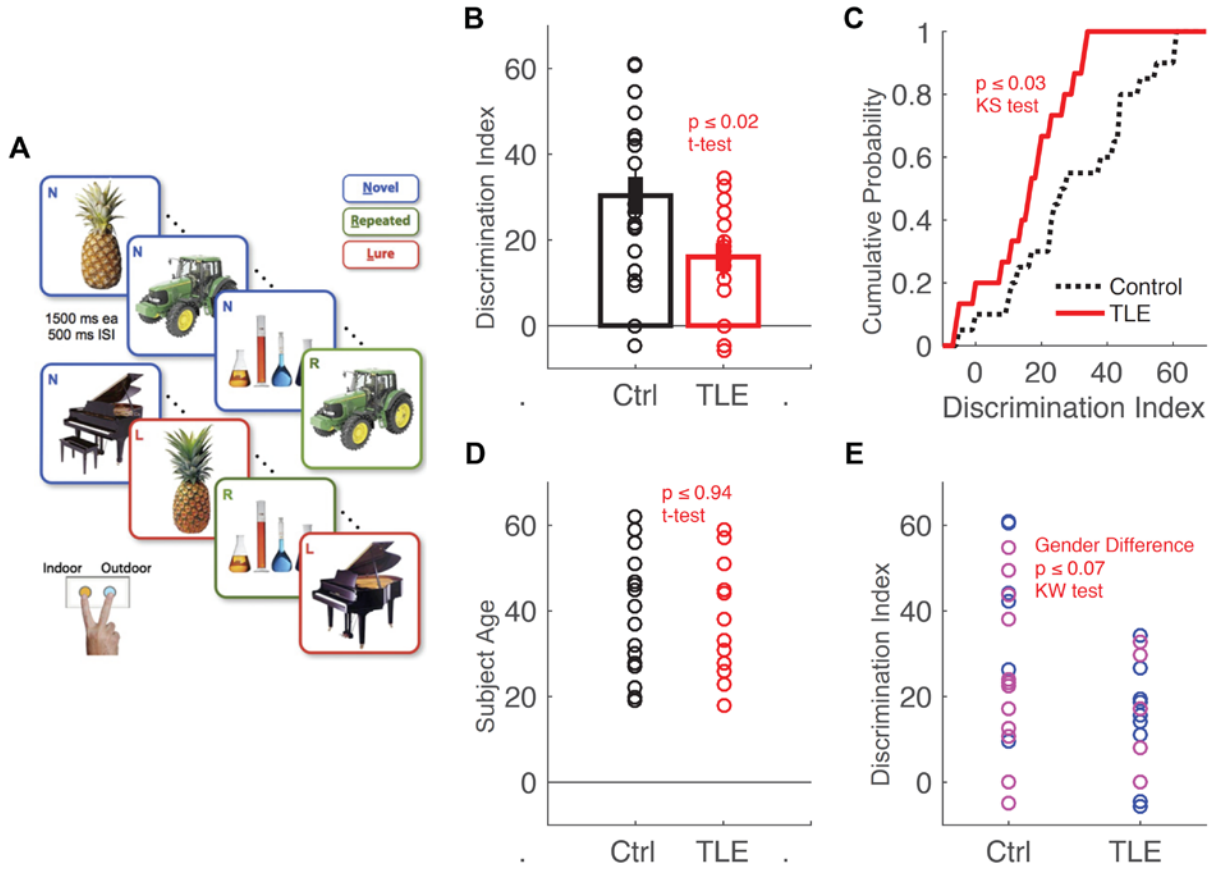


**Figure 1. Human patients with TLE have mnemonic discrimination deficits**

**(A)** A schematic (adapted with permission from Yassa et al., 2011) of the mnemonic discrimination task given to patients with TLE and nonepileptic control subjects. The discrimination index measures the ability of participants to correctly identify images as similar but not identical to a previously seen image.

**(B)** Human patients with temporal lobe epilepsy (red, n = 15) display a significant deficit in this object recognition-based mnemonic discrimination task compared to nonepileptic control subjects (black, n = 20). Unpaired two-sided T-test: P = 0.0183, T(33) = 2.4832.

**(C)** The same data from B, presented as cumulative frequency distributions. A non-parametric one-way KW ANOVA on the indices grouped by treatment confirms a highly significant deficit in visual pattern separation memory for human subjects with TLE (P = 0.0343, $\chi^2(34) = 4.4809$).

**(D)** TLE and Ctrl groups were properly age matched (unpaired two-sided T-test: P = 0.9411, T(31) = -0.0745).

**(E)** There were slightly more women than men in the control group, but the gender difference was not significant between the two treatments (one-way KW ANOVA on gender values, 1 or 2, grouped by treatment: P = 0.0663, $\chi^2(32) = 3.3724$).

To investigate the effect of TLE at the behavioral, computational and cellular levels, we turned to the common post-kainate animal model of acquired TLE (KA, **Methods – Mouse experiments**). An automated detection algorithm of interictal spikes (IISs) allowed us to quantify epileptiform activity in each animal even in the absence of seizures (**Methods – Automated EEG analysis** and see Pfammatter et al. 2018). Most KA animals developed IISs (**Figure 2**).

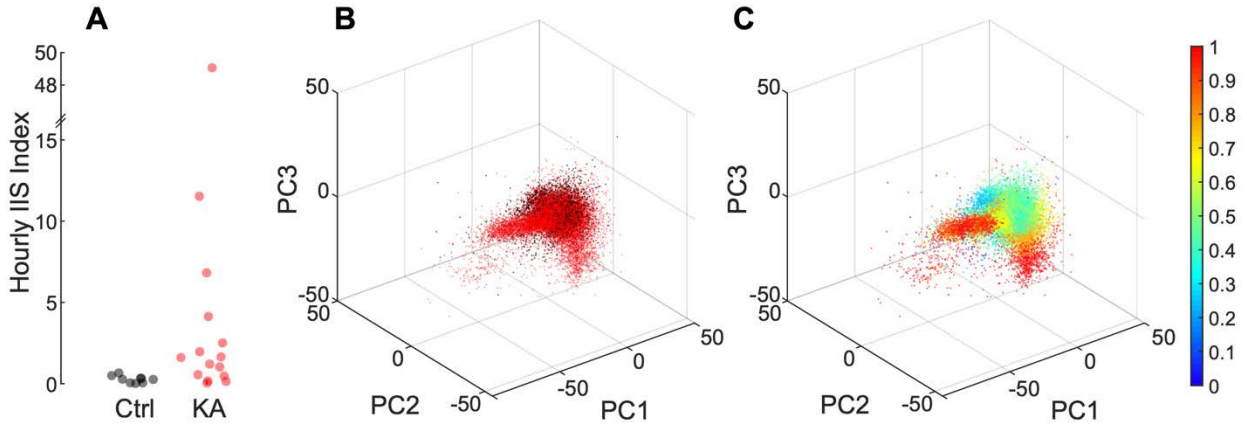


**Figure 2. Kainate-injected mice have epileptiform electrographic events with a range of event frequency**

**(A)** The Hourly Interictal Spikes (IIS) index, a proxy for epilepsy severity based on EEG recordings (Pfammatter et al., 2018), was calculated for 9 Ctrl (black) and 15 KA (red) animals. KA animals have a significantly higher Hourly IIS index than Ctrl animals (U-test: $P = 0.009$, $Z = 2.207$, rank sum = 225).

**(B)** To compute the index, high-amplitude events (200 ms duration) were identified from left frontal EEG and projected on the first three principal components (PC) of the ensemble of events from all mice. Each dot here is an EEG event, red when from a KA animal and black when from a Ctrl. Notice the 'fingers' of red KA dots extending from the central cluster of mixed Ctrl and KA data points.

**(C)** Using a voxel gridding of the PC space (voxel size: 10 cubic units), we calculated the probability for each event to be specific to KA treatment (see scale bar). The hourly IIS index of a mouse is the average number of detected events/hour, weighted by their probability of being specific to the KA treatment.

Prior to EEG recordings, mice were subjected to an object-location novelty-recognition BPS task (**Methods – Mouse Behavior**) where their ability to discriminate between a moved object versus an identical unmoved object was measured for different object displacement distances (**Figure 3A**). Our results demonstrate that, on average, KA mice have lower object-location mnemonic discrimination than control mice at all object distances (**Figure 3B-C**). Control analyses of motility (assessed by the total distance moved) and anxiety levels (assessed by the time spent near walls) revealed that KA mice have no obvious locomotor deficits nor do they spend more time near walls during the testing phases (**Figure 3D-E**). Moreover, there was no correlation between individual mnemonic discrimination ratios and total distance moved ($R^2$ = 0.028, *T(118)* = 1.86, *P* = 0.066) or time spent near walls ($R^2$ = 0.002, *T(118)* = 0.50, *P* = 0.62) during phase 3. These results suggest that differences between KA and control mice in the BPS task were not due to differences in motor ability, exploration or anxiety.

TLE is thus accompanied by mnemonic discrimination deficits in both humans and mice.

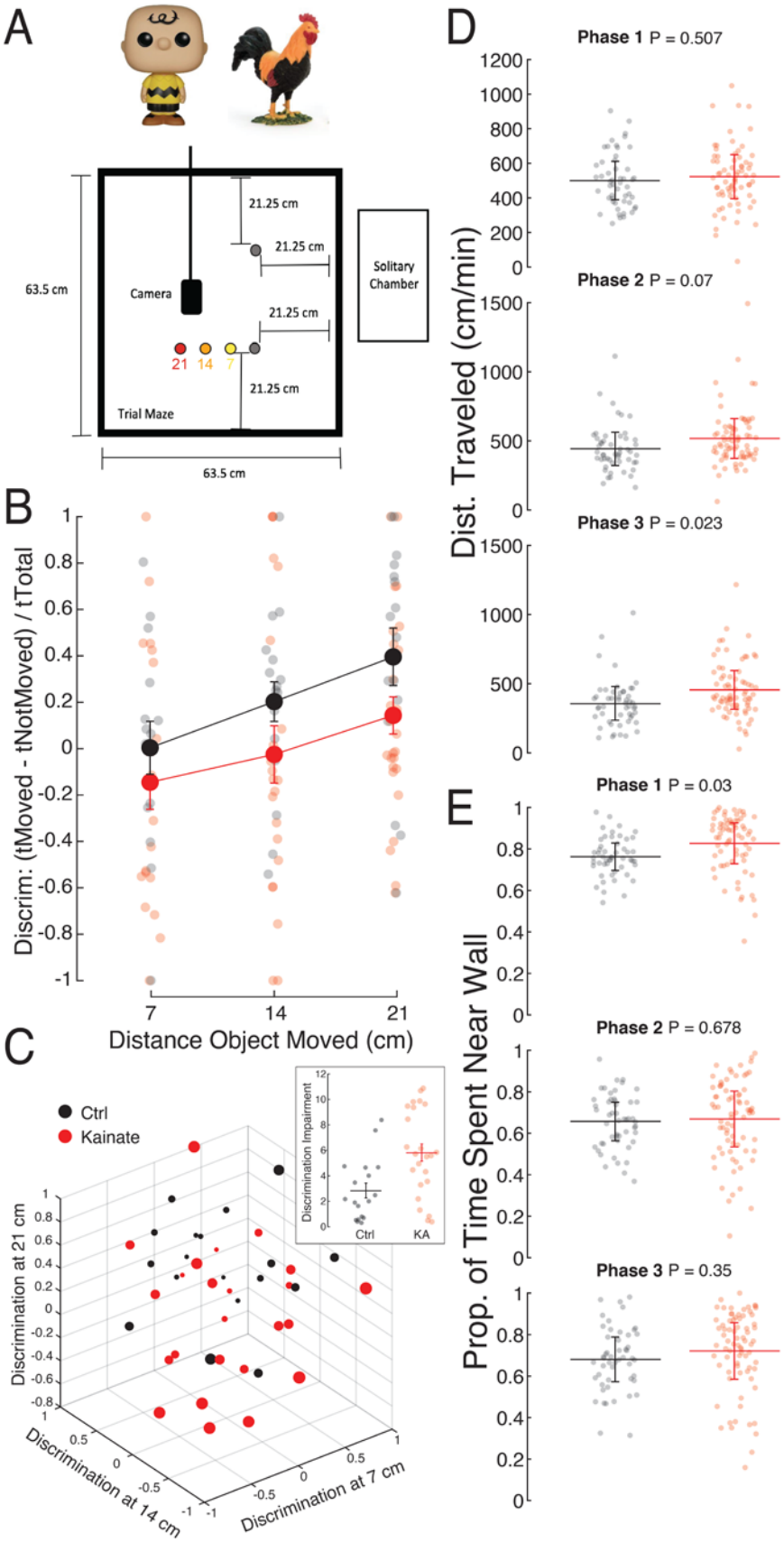

**Figure 3. Kainate-injected mice have deficits in mnemonic discrimination**

**(A)** Object location BPS task arena setup. The experiment was run in three phases of three minutes. In Phase 1, a mouse was allowed to explore the empty square arena. In Phase 2, the same mouse was allowed to explore the same arena but with two identical objects (position indicated by grey circles). In Phase 3, one randomly chosen object was moved either 7, 14 or 21 cm from its original position and the mouse was allowed to explore again. Between phases, the mouse was placed in a solitary chamber for 1.5 minutes. Each mouse performed the task once at each distance with different objects, in randomized order, with a week in between trials.

**(B)** Performance at the BPS task is evaluated with a discrimination ratio computed for each animal at each distance. Healthy mice generally prefer to explore objects with novel characteristics (such as change in relative position) and are thus expected to spend more time with the moved object if they notice it has changed location. Discrimination is thus quantified as the difference between the time exploring the moved object and the time exploring the unmoved object. A two-way ANOVA with repeated measures shows that mice discriminate better when objects are moved farther apart, and that Ctrl mice (n = 29) discriminate better than KA mice (n = 27) (Distance Object Moved: $P = 0.002$, $F(1,118) = 9.84$; Treatment: $P = 0.027$, $F(1,118) = 5.02$).

**(C)** Subset of the data in B plotted in the space of discrimination at each distance, allowing a clearer picture of individual performance. Each animal is represented by a single dot in this 3D space (42 animals with records at the three distances: 24 KA and 18 Ctrl). For each data point, the Mahalanobis distance (De Maesschalck et al., 2000) from the Ctrl centroid is represented by the dot size, and is also displayed in the inset (mean +/- SEM). Mahalanobis distances are larger for KA than Ctrl animals, confirming that the KA population displays mnemonic discrimination deficits (two-sided T-test: $P = 0.003$, $T(40) = -3.15$).

**(D,E)** Control analysis to determine whether there were motor impairments or anxiety/curiosity differences between KA and Ctrl mice, across phase 1, 2 and 3 of the BPS task. In each panel, individual mice are represented by one to three data points, as in B, depending on how many conditions (Distance Object Moved) they were tested on. Mean +/- SEM.

**(D)** Distance traveled was used as a proxy for motor ability. During Phase 1 and Phase 2, control and KA mice moved similar distances ($P = 0.507$, $F(1, 120) = 0.443$ and $P = 0.070$, $F(1, 122) = 3.35$). During Phase 3 KA mice moved farther than Ctrl mice ($P = 0.023$, $F(1, 124) = 5.34$).

**(E)** Percent of time near wall was used as a proxy for anxiety. During Phase 1 (habituation), KA animals spent more time near the maze walls compared to Ctrl ($P = 0.03$ $F(1,120) = 4.82$). During Phases 2 and 3, Ctrl and KA animals spent a similar amount of time near walls ($P = 0.68$, $F(1,122) = 0.173$ and $P = 0.35$, $F(1, 124) = 0.881$). F-tests correspond to one-way ANOVAs with repeated measures, with Treatment as a categorical fixed effect.

***DG computational impairments in TLE.*** To test our hypothesis that DG pathologies in TLE lead to a breakdown of the neural pattern separation function of the DG, which in turn would translate into the cognitive impairments we observed, we measured pattern separation in hippocampal slices from the same KA and control mice used above in behavioral and EEG

experiments. Briefly, the assay has three steps (**Figure 4A-B** and see Madar et al. 2019a, b): 1) ensembles of stimulus patterns (simulating afferent input spiketrains) are generated, with known degrees of similarity to each other. These spiketrains are then fed into the DG by stimulating the lateral perforant path. 2) The response of a single GC is recorded in whole-cell current-clamp. 3) The similarity between the output spiketrains is compared to the similarity between the input spiketrains, revealing the degree of separation or convergence (**Figure 4C** and see **Material and Methods – Neural pattern separation analysis**).

We tested pattern separation levels in response to three types of input sets. Input sets of type 1 were constituted of Poisson spiketrains with a 10 Hz mean firing rate designed to have a prespecified average similarity as measured by the Pearson's correlation coefficient (R) (**Figure 4B**). For an input set with spiketrains correlated by 77% between each other (timescale: $\tau_w$ = 20 ms), the output spiketrains of GCs from epileptic mice had a higher average correlation ($R_{output}$) than GCs from control mice (**Figure 4C**). This demonstrates a decrease in pattern separation in the DG of epileptic mice. Exploring a wider range of input correlations shows that the pattern separation function of the DG of KA mice is generally impaired compared to the normal pattern separation function (**Figure 4D**). Furthermore, a decrease in pattern separation was observed at multiple timescales (millisecond to second) and using multiple similarity metrics that assume different neural codes (**Figure 4E**, see **Material and Methods – Neural pattern separation analysis**). The impairment is most noticeable using the NDP metric, showing that DG output patterns are less orthogonalized in KA animals at all timescales, whereas differences in pattern separation via scaling (SF metric) are small but significant at large timescales.

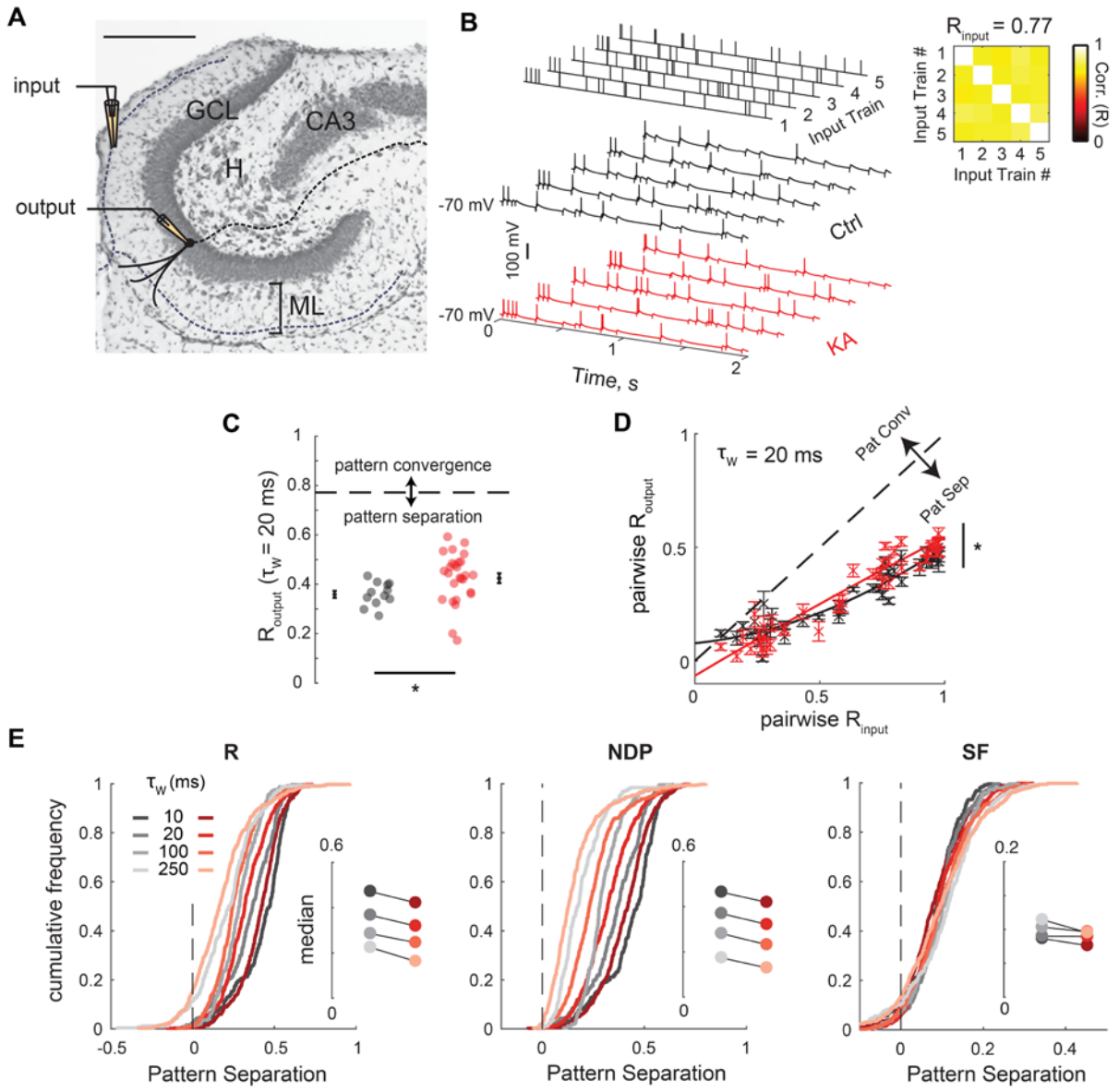


**Figure 4. Epileptic mice have neural pattern separation deficits**

**(A)** Histology of the DG in a horizontal slice (Cresyl violet/Nissl staining; scale bar: 250 µm), overlaid with a schematic of the experimental setup: a theta pipette in the ML is used to focally stimulate the outer molecular layer (input) while a responding GC is recorded via whole-cell patch-clamp (output). GCL: granule cell layer, H: hilus, ML: molecular layer. Solid lines represent dendrites and dashed lines axons.

**(B)** Current-clamp recordings of the membrane potential of two different GCs (Ctrl and KA) in response to the same set of input trains. An input set is constituted of five different trains of electrical pulses following a Poisson distribution with an average rate of 10 Hz. The Pearson's correlation coefficient (R) between two input trains is computed with a binning window ($\tau_w$) of 20 ms (*Left*). $R_{input}$ is the average of the ten pairwise coefficients, diagonal excluded. After converting the GC recordings to vectors of binned spike counts, the pairwise coefficients and their average ($R_{output}$) can be computed the same way (Madar et al, 2019b). Note that the input set was repeated 10 times to yield output sets of fifty sweeps (only one repeat is shown).

**(C)** The $R_{output}$ of GCs from kainate-injected animals is higher, on average, than in GCs from controls. Data points correspond to single output sets (KA: 27 recordings from 24 GCs; Ctrl: 12 recordings from 11 GCs), all being responses to the same input set as in B. Black crosses with error bars are means +/- SEM. The asterisk signals significance: U-test comparing the medians: P = 0.011, Z = -2.541, rank sum = 156; two-sided two-sample KS test comparing the distribution shapes: P = 0.0037, D = 0.583. The dashed line corresponds to $R_{input}$ (0.77): any value below the line implies effective pattern separation. Thus, GCs from kainate animals exhibit less pattern separation than controls.

**(D)** Pattern separation was investigated over a wide range of input correlations by using four different input sets of five 10 Hz Poisson trains (at $\tau_w$ = 20 ms: $R_{input}$ = 0.24, 0.45, 0.77, 0.95). Crosses and error bars correspond to mean +/- SEM (pw $R_{input}$, pw $R_{output}$) across multiple recordings (KA: 6-24 GCs per input set; Ctrl: 4-11 GCs). Data points below the identity line (dashed) correspond to pattern separation. The distributions between KA and Ctrl are significantly different (ANCOVA with separate parabolic models fitting the data points and not the means: P < 0.0001, F(3,714) = 15.485. Solid curves are the parabolic models used for the ANCOVA.

**(E)** Levels of pattern separation measured using different similarity metrics (S: R, NDP and SF, see Methods) and timescales. Cumulative frequency distributions of the distance of (pw $S_{input}$, pw $S_{output}$) data points to the identity line in pattern separation graphs like in E. Positive values of the x-axis correspond to pattern separation, and negative values to pattern convergence. Insets show medians. For R and NDP, distributions are significantly shifted to the left, showing that GCs from KA exhibit less decorrelation and less orthogonalization (ANCOVA as in D, but using separate linear models: P < 0.01 for $\tau_w$ = 5 to 1000 ms. For R/NDP and $\tau_w$ = 10, 20, 100, 250 ms, P = <0.0001/<0.0001, <0.0001/<0.0001, 0.001/<0.0001, 0.011/0.0001, F(2, 716) = 15.2/18.2, 20.3/23.4, 6.87/15.97, 4.5/9.4). For SF, scaling levels are weakly but significantly shifted to less separation at large $\tau_w$ (SF: P > 0.2 except at 250 ms and 500 ms, with P = 0.026, 0.046, F(2, 716) = 3.65, 3.09 respectively).

An input set of type 2, made of Poisson spiketrains similar in terms of R but with varying firing rates (**Figure 5A1**), and an input set of type 3, with 10.5 Hz uncorrelated trains (R = 0) with varying burstiness (**Figure 5B1**), were designed to explore a wide range of input similarities as measured by SF and to characterize DG computations on inputs with a variety of statistical structures (Madar et al., 2019b). As we have shown before, the normal DG exhibits low pattern separation via scaling for highly similar inputs, and significant pattern convergence for dissimilar inputs (Madar et al., 2019b). In KA mice, GCs show a decrease in both pattern convergence and separation via scaling: the DG computation function is steeper, closer to the identity line, meaning that the DG of KA mice is weaker at transforming the similarity of its inputs in general

509 (**Figure 5A1 and B1**). When similarity is measured with R or NDP (binwise synchrony code)
510 instead of SF (neural code focused on FR and bursting), these experiments confirmed that pattern
511 separation is decreased in TLE (**Figure 5A2**) and that this deficit is strongest when inputs are
512 highly similar (i.e., when pattern separation is theoretically most important) and weaker when
513 inputs are already dissimilar (**Figure 5B2**).
514

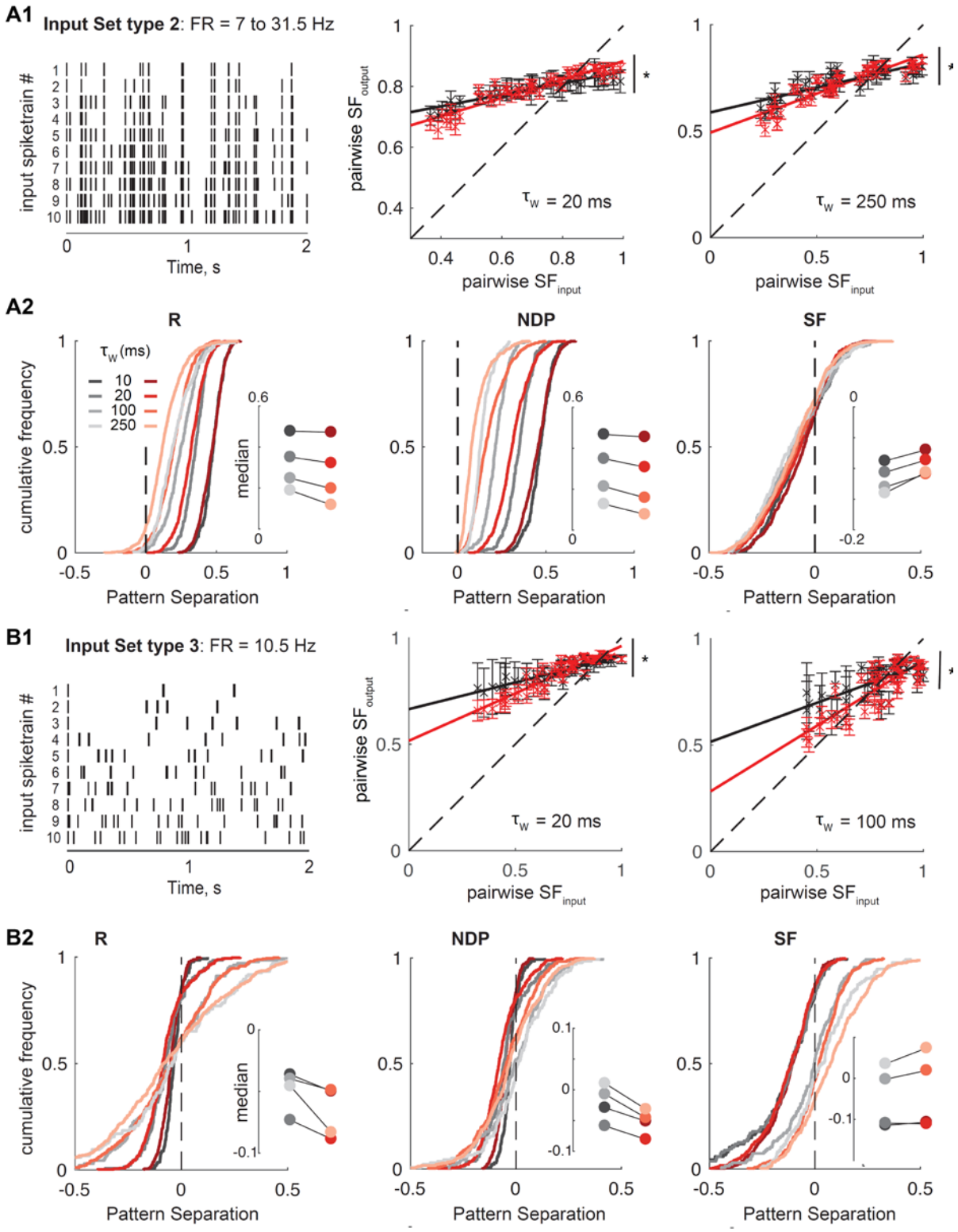


**Figure 5. Multiple DG computations are affected by epilepsy**

Our standard input sets (type 1, Figure 4) consisted of 10 Hz Poisson trains. Two other input sets (type 2 and 3) were designed to explore single GCs responses to inputs with diverse structures

and statistics, both with a wide range of pairwise similarity as measured by SF (in contrast to input sets of type 1).
**(A1)** *Left*: Input set type 2 was constituted of spiketrains following a Poisson distribution, each with a different firing rate (FR), but with an average $R_{input}$ constrained around 0.75 ($\tau_w$ = 10 ms). *Middle and Right*: Pattern separation graphs showing the pairwise output spiketrain similarity as a function of the pairwise input similarity, as measured by SF with two different timescales, averaged across multiple GCs (KA: 16, Ctrl: 5). Distributions are significantly different, suggesting in particular that epilepsy causes a decrease in pattern convergence (via scaling) for low input similarities (ANCOVA with separate linear models, for $\tau_w$ = 20 and 250 ms respectively : P = 0.0016 and < 0.0001, F(2, 941) = 6.5 and 10.4). **(A2)** Levels of pattern separation for type 2 inputs, measured using different similarity metrics and timescales as in Figure 4. It confirms that epilepsy decreases the separation of similar Poisson input spiketrains as measured by R and NDP, consistent with Figure 4, and shows that differences in terms of SF, although small, are significant (ANCOVA as in A1: R: P < 0.0001 for $\tau_w$ = 20 ms up to 1000 ms, P = 0.02 and 0.18 for 5 and 10 ms; NDP and SF: P < 0.025 for $\tau_w$ up to 1000 ms. Detailed statistics for $\tau_w$ = 5, 10, 20, 50, 100, 250, 500 and 1000 ms respectively: R, P = 0.0243, 0.1820, <0.0001, <0.0001, <0.0001, <0.0001, <0.0001, <0.0001, F(2, 941) = 3.7, 1.7, 10.2, 15.1, 24.1, 36.0, 50.2, 27.0; NDP, P = 0.0022, 0.0240, <0.0001, <0.0001, <0.0001, <0.0001, <0.0001, <0.0001, F(2, 941) = 6.2, 3.7, 13.8, 17.4, 21.4, 26.0, 21.0, 16.8; SF, P = 0.0002, 0.0012, 0.0016, 0.0240, 0.0073, <0.0001, <0.0001, 0.0002, F(2, 941) = 8.7, 6.7, 6.5, 3.7, 4.9, 10.9, 10.4, 8.7).
**(B1)** *Left:* Input set type 3 was constituted of spiketrains with 21 spikes (FR = 10.5Hz) that were distributed among bins to produce trains with varying burstiness (Madar et al., 2019b). R is close to 0 for all pairs. *Middle and Right*: same analysis as in A1 (KA: 8 GCs, Ctrl: 3 GCs). Distributions are significantly different, suggesting again that epilepsy causes a decrease in pattern convergence via scaling, for low input similarities (ANCOVA for $\tau_w$ = 20 and 100 ms: P < 0.0001 and F(2, 491) = 10.3 and 13.8 respectively).
**(B2)** Same analysis as in A2. The directions of impairments are the same as in A2, showing that epilepsy decreases pattern separation in terms of R and NDP but slightly improves it in terms of SF. The shift via scaling is weak but significant at all timescales, and larger at the longest $\tau_w$. ANCOVA: R, P < 0.05 for $\tau_w$ = 5, 10 and 500 ms; NDP and SF, P < 0.007 for $\tau_w$ up to 500 ms. Detailed statistics for $\tau_w$ = 5, 10, 20, 50, 100, 250, 500 and 1000 ms respectively: R, P = 0.0451, 0.0004, 0.3727, 0.7357, 0.9340, 0.4271, 0.0012, 0.2889, F(2, 491) = 3.1, 8.1, 1.0, 0.3, 0.1, 0.8, 6.8, 1.2; NDP, P = <0.0001, <0.0001, 0.0003, 0.0012, <0.0001, 0.0069, <0.0001, 0.4154, F(2, 491) = 11.1, 24.3, 8.4, 6.8, 11.2, 5.0, 14.6, 0.9, SF, P = <0.0001, <0.0001, <0.0001, <0.0001, <0.0001, 0.0065, 0.0002, 0.0003, F(2, 941) = 42.1, 20.9, 10.3, 13.6, 13.8, 5.1, 8.5, 8.1.

***Pathological spiking patterns in a subset of GCs from epileptic mice.*** What features of GC output spiketrains are changed in TLE to explain the difference in DG computations between KA and control mice? On visual inspection, we noticed that many KA neurons occasionally fired short bursts of action potentials after a single input pulse (**Figure 6A**), which is quite unusual for control GCs (Madar et al., 2019a). To determine whether there was a difference in the spiking

patterns of KA and control GCs, we measured three spiketrain features: 1) the average firing rate (FR) of a GC across a full recording set (fifty spiketrains), 2) the probability of spiking after a single input pulse (SP) and 3) the probability of bursting (p(Burst), i.e., more than one spike) after a single input pulse. Our results show that on average GCs from KA mice fire more faithfully after an input (**Figure 6B**) and also tend to fire in bursts (**Figure 6C-D**), which together lead to a higher FR (**Figure 6B, E**).

Closer inspection suggests that the distributions of SP, p(Burst) and FR are different between KA and controls, with larger variance and upper tails for GCs from KA mice **(Figure 6B-E).** Although we did not formally test for discrete clusters, visual inspection of Figure 6E shows that a subset of GCs from KA animals have higher SP, p(Burst) and FR than any control GC. Thus, it appears that, following an epileptogenic insult, only a subset of GCs displayed pathological characteristics amidst a background of seemingly normal GCs.

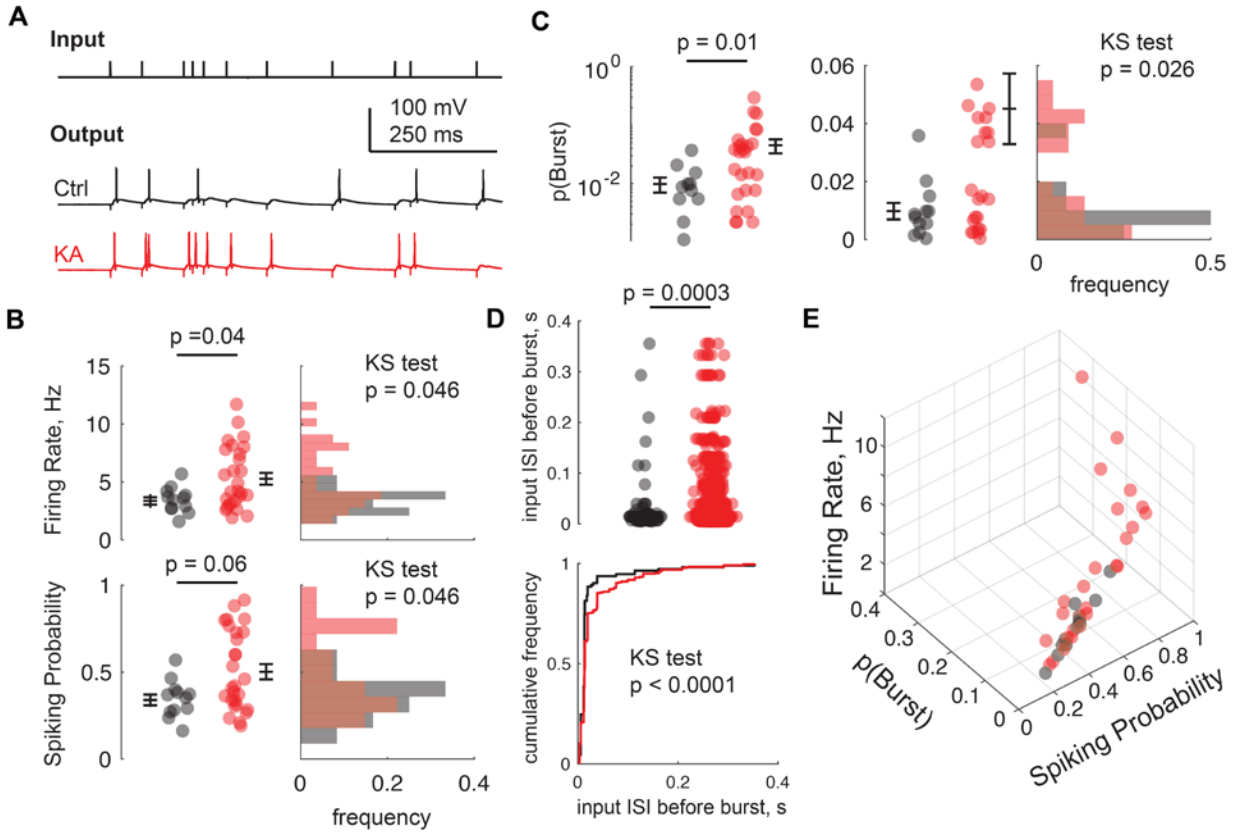


**Figure 6. In epileptic mice, a subpopulation of GCs shows pathological spiking patterns**

**(A)** Example of current-clamp recordings in GCs from a kainate-injected (KA) vs a control animal in response to the same Poisson input train, illustrating that some GCs from KA spiked more, and had a tendency to fire short bursts (2-4 spikes riding a single EPSP).

**(B-E)** Some GCs from KA exhibited larger firing rates due to a higher probability of spiking at least once after an input spike (spiking probability), and sometimes a higher probability of spiking more than once between two input spikes ( p(Burst) ) than GCs from controls. The firing rate, spiking probability and p(Burst) of a neuron were all computed as the average over the fifty sweeps of an output set from a pattern separation experiment (input set type 1, see Figure 4B).

**(B)** *Left*: data points correspond to the same recordings as in Figure 4C (KA: 27; Ctrl: 12). Black dash and error bars are mean +/- SEM. A U-test was used to compare the medians, showing that on average FR and SP are higher in KA (FR: P = 0.0415, Z = -2.04, rank sum = 172.5; SP: P = 0.0613, Z = -1.87, rank sum = 168.5). *Right*: Frequency distributions of the same data. A one-sided two-sample KS test shows that the KA distribution has a larger tail in both cases (FR and SP: P = 0.0465, D = 0.4074), indicating that a subset of KA GCs are pathological.

**(C)** Same as in B for p(Burst). Note that the left graph has a $\log_{10}$ scale showing all data points, whereas the middle graph has a linear scale zoomed in (i.e. not showing the 5 largest KA values). The graph on the right has the same scale as the middle graph. Together, they suggest that in KA, there might be a healthy population of GCs coexisting with a different population of pathologically bursty GCs (U-test: P = 0.0153, Z = -2.16, rank sum = 168.5; KS test: P = 0.0259, D = 0.4444).

**(D)** Some bursts were detected by our algorithm in GCs from Ctrl mice, but the vast majority of those were due to the temporal summation of two EPSPs resulting from input spikes occurring close in time. In contrast, a large number of bursts in GCs from KA mice come after an isolated

input spike. *Top*: Time interval between the two input spikes (inter-spike-interval, ISI) preceding a given burst. Data points correspond to all detected bursts from the recordings in C. U-test: P = 0.0003, Z = -3.58, rank sum = 5906.2. *Bottom*: Cumulative frequency distributions of the same data. A one-sided two-sample KS test demonstrates that the distributions are different (P < 0.0001, D = 0.2699).
**(E)** Same data as in B and C: the elbow in the distribution of SP, p(Burst) and FR values visually defines two clusters of neurons. One cluster contains GCs from both KA and Ctrl mice (with GCs from both groups spanning a large range of SP values but low p(Burst)) and can be considered "normal". In contrast, the other cluster, with highest SP combined with high p(Burst), contains only GCs from KA animals and can thus be considered "pathological".

What is the origin of the pathological spiking patterns? We first controlled that stimulation intensities were comparable between treatment groups and were not causative of abnormal spiking patterns (**Figure 7A**). We next asked whether the abnormal firing came from changes in the synaptic drive. To answer this question, we measured the synaptic input-output relation (Ewell and Jones, 2010) by recording GCs first under current-clamp then under voltage-clamp, in response to the same pattern separation stimulus protocol (**Figure 7B1-2**). Our data show that the average excitatory drive per neuron was not different between KA and control groups, and that it does not predict burstiness (**Figure 7B3**). A finer grained analysis on the individual currents suggests that although the excitatory drive and the spiking output are correlated, high amplitude EPSCs are neither sufficient nor necessary to elicit a burst (**Figure 7B4**). Bursting does not seem to result from other changes in excitatory input-output coupling either (**Figure 7B5**), which suggest that inhibition might be involved. GCs are indeed subjected to strong tonic, feedforward and feedback inhibition that controls the sparseness of their activity (Coulter and Carlson, 2007; Ewell and Jones, 2010; Pardi et al., 2015; Lee et al., 2016) and is altered in TLE (Alexander et al., 2016; Dengler and Coulter, 2016). We did not record evoked IPSCs directly but, in normal mice, partial block of inhibition elevates GC firing rates and causes bursts (Madar et al., 2019b) similar to what we observed here in KA mice. All our results thus

converge to support the hypothesis that pathological spiking arises from an excitation/inhibition imbalance in a subset of GCs, likely driven by a decrease in inhibition.

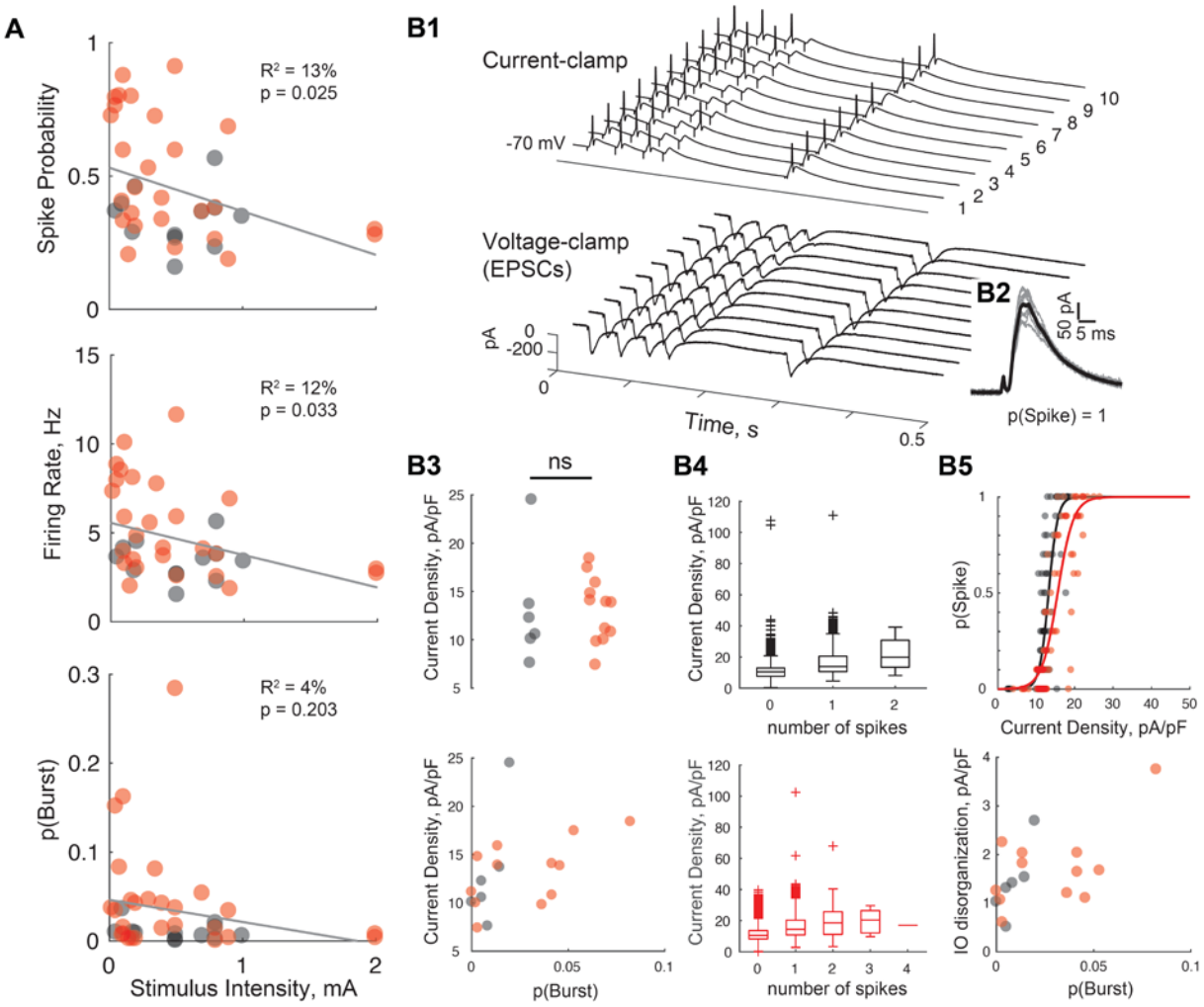


**Figure 7. Pathological bursting arises from an excitation/inhibition imbalance**

**(A)** Bursting and high firing rates were not an artefact of stimulation differences: The current intensity of the electric stimulation did not significantly differ between KA and Ctrl (same recordings as in Figure 4C and 6B-E, U-test: P = 0.2991, Z = 1.04, rank sum = 274.5) and stimulus intensity was a poor predictor of pathological firing patterns (as indicated by the low $R^2$ values of linear regressions. For FR/SP/pBurst: $R^2$ = 12.75%/11.69%/4.35%, F(2,37) = 5.4/4.9/1.7, P = 0.0257/0.0332/0.2027).

**(B)** For a subset of neurons in A (KA: 12; Ctrl: 6), we followed the current-clamp recording with a voltage-clamp recording ($V_{hold}$ = -70mV) in response to the same pattern separation protocol in order to assess the excitatory synaptic drive and its relationship with spiking behavior. The stimulus electrode location and current intensity was unchanged. **(B1)** Example of current-clamp (top) and voltage-clamp (bottom) recording in the same GC from a Ctrl animal. Only the first

500 ms of the ten responses to repetitions of the first input train shown in Figure 4B are displayed. *Top*: action potentials are truncated at 0 mV. *Bottom*: stimulation artefacts and occasional unclamped spikes were blanked. **(B2)** The ten EPSCs (grey) associated to first pulse of input trains in B1 and the mean EPSC (black). We assessed the excitatory drive as the maximum inward current in the interval between each input pulse minus the current baseline (i.e., mode of the current over the full sweep). P(Spike) was defined as the probability of spiking during this interval across the ten sweeps of the current-clamp recording. **(B3)** *Top*: The mean EPSC density for each neuron was not significantly different between KA and Ctrl (U-test: P = 0.5532, rank sum = 50; two-sided two-sample KS test: P = 0.1935, D = 0.4167), suggesting that pathological spiking cannot be explained by larger EPSCs in KA mice. *Bottom*: Indeed, no clear relationship exists between p(Burst) and the mean current density, as some GCs with a great synaptic drive do not exhibit much bursting, and vice versa. **(B4)** Consistently, the peak current density associated to each inter-input-interval in a recording is not well correlated to the corresponding number of spikes in the current-clamp trace, for both Ctrl (top) and KA (bottom). For example, excitatory currents of the same magnitude can be associated to 0, 1, 2, 3 or 4 spikes. EPSC amplitude is thus not sufficient to explain the spiking output, which suggests that other factors, like reduced inhibition, are likely implicated in causing pathological bursts. **(B5)** *Top*: The average EPSC density between two input spikes is plotted against the corresponding probability of spiking p(Spike), as in Ewell and Jones (2010). The resulting input-output (IO) distribution is fitted with a sigmoid (two GCs representative of KA and Ctrl are shown). *Bottom*: In a subset of GCs, mostly from KA, The IO distribution appears disorganized and sometimes difficult to fit. A nonparametric proxy of this disorganization is the standard deviation (SD) of the current density, averaged across each level of p(Spike) excluding p(Spike) = 0 and 1. The average SD for a given GC was plotted against the propensity of that neuron to fire bursts. There is no clear relationship between these two quantities, suggesting that: 1) decoupling between the excitatory drive and spiking probability is not directly related to bursting and 2) a subset of GCs from KA with apparently healthy spiking patterns could already exhibit a more subtle but pathological IO disorganization.

How do high FR and bursts relate to the DG computational impairment measured in KA mice? We first tested the hypothesis that higher GC firing rates and burstiness yield less pattern separation as measured with R (**Figure 8A**). In GCs of young mice, FR and pattern separation are related, but loosely (Madar et al., 2019a), whereas here in adult mice there is a strong linear relationship, such that GCs with pathologically high FR exhibit pathologically low pattern separation. Similarly, abnormal bursting corresponds to abnormally low levels of pattern separation. This analysis relates cell-wise spiking features (FR or pBurst averaged across all

678 spike trains of a recorded neuron) to a form of pattern separation that is not theoretically
679 concerned with such features (Madar et al., 2019b).

680 Other forms of pattern separation, more directly related to FR or bursting, can in theory
681 also be performed: for example by increasing spiketrain-to-spiketrain *variability* in FR or
682 burstiness of the output neuron, even if the average quantities were identical (Madar et al.,
683 2019b). Because pathological GCs only occasionally fired bursts, we asked whether TLE could
684 affect such forms of pattern separation. To test this, we measured the spiketrain-to-spiketrain
685 variability in FR as well as in two complementary measures of burstiness (occupancy and
686 compactness, see **Materials and Methods – Neural pattern separation analysis**). For input
687 sets of type 1 (10 Hz Poisson), GC output variability was slightly lower in terms of burstiness or
688 FR. This weak type of pattern convergence disappeared in GCs from KA mice (**Figure 8B**). For
689 input sets of type 2 and 3, no significant difference between KA and Ctrl was detected (**Figure**
690 **8C-D**). Overall, Figure 8 suggests that TLE reduces DG neural pattern separation mostly by
691 raising average levels of FR and burstiness, rather than through spiketrain-to-spiketrain
692 variations of those features.

693

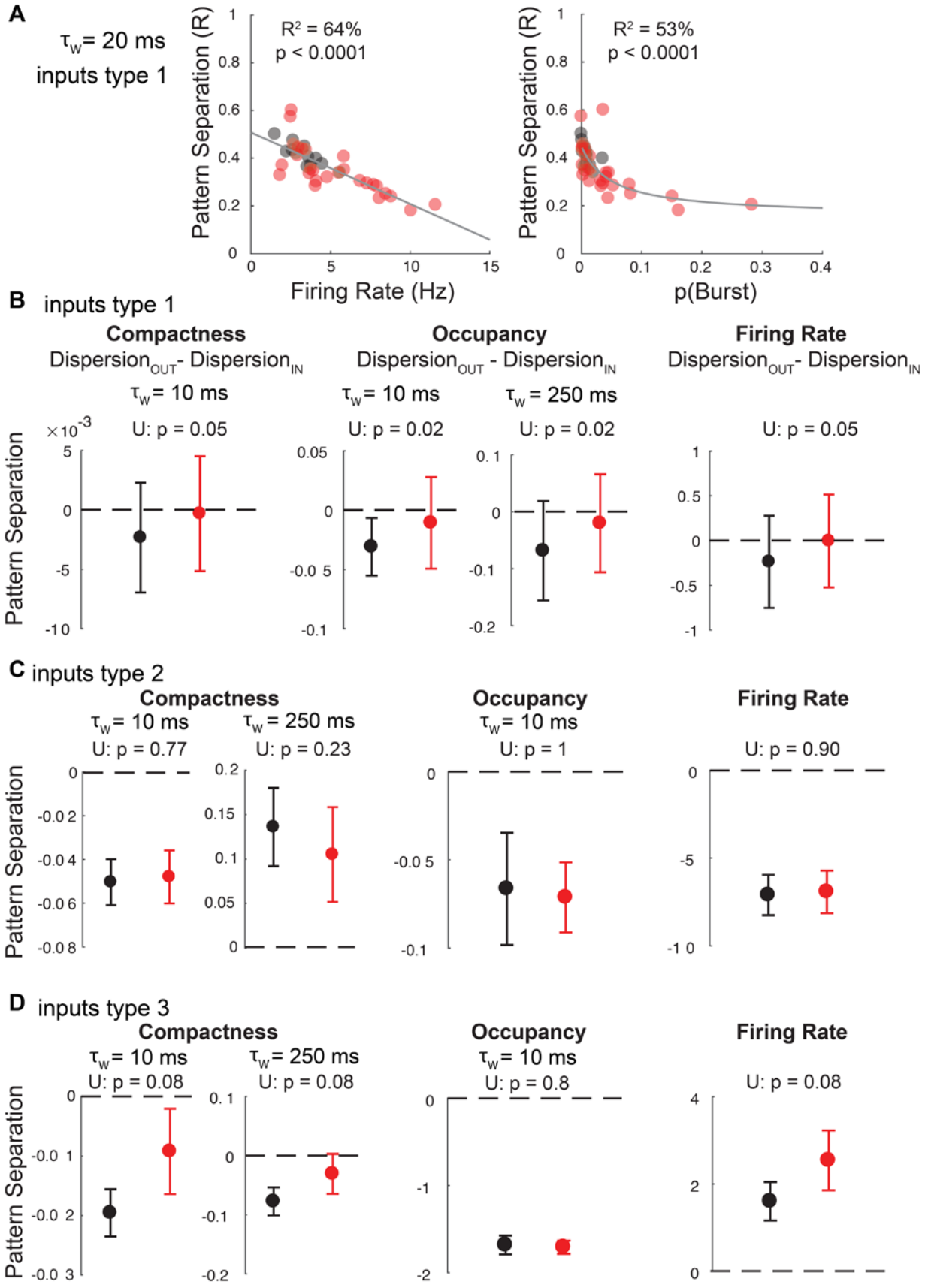


694

**Figure 8. Pathological spiking patterns explain pattern separation differences in epilepsy**
**(A)** Neurons with high average firing rates and burstiness exhibit lower pattern separation (computed as $R_{input} - R_{output}$). Same data as in Figure 4C and 6B-C. There is a strong linear relationship between firing rates and decorrelation (Grey line, $R^2 = 63.68\%$, $F(2,37) = 64.9$, $P < 0.0001$). The relationship between p(Burst) and decorrelation is better described by an inverse function with a horizontal asymptote (see Methods – Software and statistics): $R^2 = 53.1\%$, $R^2$ adjusted for 3 parameters = 50.5%, $F(3,36) = 20.4$, $P < 0.0001$.
**(B-D)** Mean +/- SEM pattern separation levels across recordings when considering burstiness codes (Compactness or Occupancy) or a rate code (spiking frequency across a 2s sweep) instead of the binwise synchrony code assumed by R. Compactness is the proportion of time bins with at least one spike, whereas occupancy is the average number of spikes in a bin. Pattern separation corresponds to more dispersion in compactness, occupancy or firing rate in the output spiketrains than the input spiketrains. Negative values mean there is pattern convergence. U-tests comparing medians of GCs from KA and Ctrl groups were performed (p-values in panel).
**(B)** In response to input sets of type 1 (10 Hz Poisson trains, same recordings as in A and Figure 4), GCs exhibit low levels of convergence, if any, in terms of compactness, occupancy and rate codes, and these levels are slightly but significantly shifted to less convergence in GCs from KA for $\tau_w$ = 10 ms. This means that the relationships between firing rate or burstiness and pattern decorrelation observed in A is not due to variations of the firing rate or burstiness across sweeps. Detailed statistics at 10, 20, 50, 100, 250 ms, Compactness: P = 0.0482, .1892, .1628, .2925, .7584, Z = -1.97, -1.97, -1.31, -1.39, 0.31, rank sum = 745, 745, 801, 794, 939 ; Occupancy: P = 0.0177, 0.2586, 0.3624, 0.1425, 0.0211, Z = -2.37, -1.13, -0.91, -1.47, -2.31, rank sum = 712.5, 816.5, 835, 788, 717; FR: P = 0.0553, Z = -1.92, rank sum = 750.
**(C)** In response to an input set of type 2 (Poisson trains with different firing rates, same recordings as in Figure 5A), GCs from KA and Ctrl do not show significant differences (P > 0.2 for all timescales and codes). Detailed statistics at 10, 20, 50, 100, 250 ms, Compactness: P = 0.7726, 0.7726, 0.8365, 0.9014, 0.2312, Z = -0.29, -0.29, -0.21, 0.12, 1.20, rank sum = 51, 51, 52, 57, 70; Occupancy: P = 1, 1, 0.9671, 0.5915, 0.2006, Z = 0, 0, 0.04, -0.54, -1.28, rank sum = 55, 55, 56, 48, 39; FR: P = 0.9014, Z = -0.12, rank sum = 53.
**(D)** In response to an input set of type 3 (10 Hz trains with varying compactness and occupancy, same recordings as in Figure 5B), GCs exhibit convergence in terms of compactness and occupancy and separation in terms of rate codes. Only computations in terms of compactness and firing rate are mildly shifted in GCs from KA for $\tau_w$ = 10 ms. Detailed statistics at 10, 20, 50, 100, 250 ms, Compactness: P = 0.0848, rank sum = 9; Occupancy: P = 0.8, 0.7758, 0.9212, 0.3758, 1, rank sum = 19.5, 20, 17, 23, 18; FR: P = 0.0848, rank sum = 9.

***Electrographic, behavioral and computational pathologies in individual mice.*** We have shown that, on average, KA mice develop EEG abnormalities (**Figure 2**), suffer mnemonic discrimination impairments (**Figure 3**) and have a bursting subpopulation of GCs with pattern separation deficits (**Figures 4-8**). Because we often performed all of the aforementioned experiments in the same mice, we next asked how those different epilepsy-related pathologies

736 are linked at the individual level (**Figure 9**). In a simple framework where behavioral
737 impairments are caused by computational deficits that are due to reorganization of DG network
738 function that also leads to an increase in epileptiform EEG events, one could expect a simple
739 relationship between all the variables we measured. Interestingly, our data suggest a more
740 complex view. For example, animals with few interictal spikes may still harbor some
741 pathological neurons (**Figure 9A**) and be highly impaired at the BPS task (**Figure 9B**). This
742 shows that both DG network pathologies and mnemonic impairments can occur independent of,
743 or before, early EEG abnormalities. Inversely, both normal and pathological GCs were recorded
744 in mice with more advanced EEG pathology, which confirms that those two subpopulations can
745 coexist in the same KA animal (**Figure 9A**). Mice with clearly epileptiform EEG activity can
746 also sometimes perform normally on the BPS task (**Figure 9B**). The variability in individual
747 behavior and in cell sampling prevents us to definitively conclude on the relationship between
748 single-cell pattern separation and mnemonic discrimination but, importantly, KA animals with
749 the largest cognitive impairments all had at least one pathological recorded GC (**Figure 9C**).
750 Finally, in cases where EEG, BPS and patch-clamp data were all obtained from each animal, the
751 combination of these measurements yielded a very obvious separation between normal and KA
752 subjects. Overall, our results suggest that epilepsy-related pathologies do not all develop in
753 concert and that computational, behavioral and electrographic measures provide complementary
754 informative dimensions that, together, better assess the epileptic state than any single dimension
755 or pair of dimensions.
756

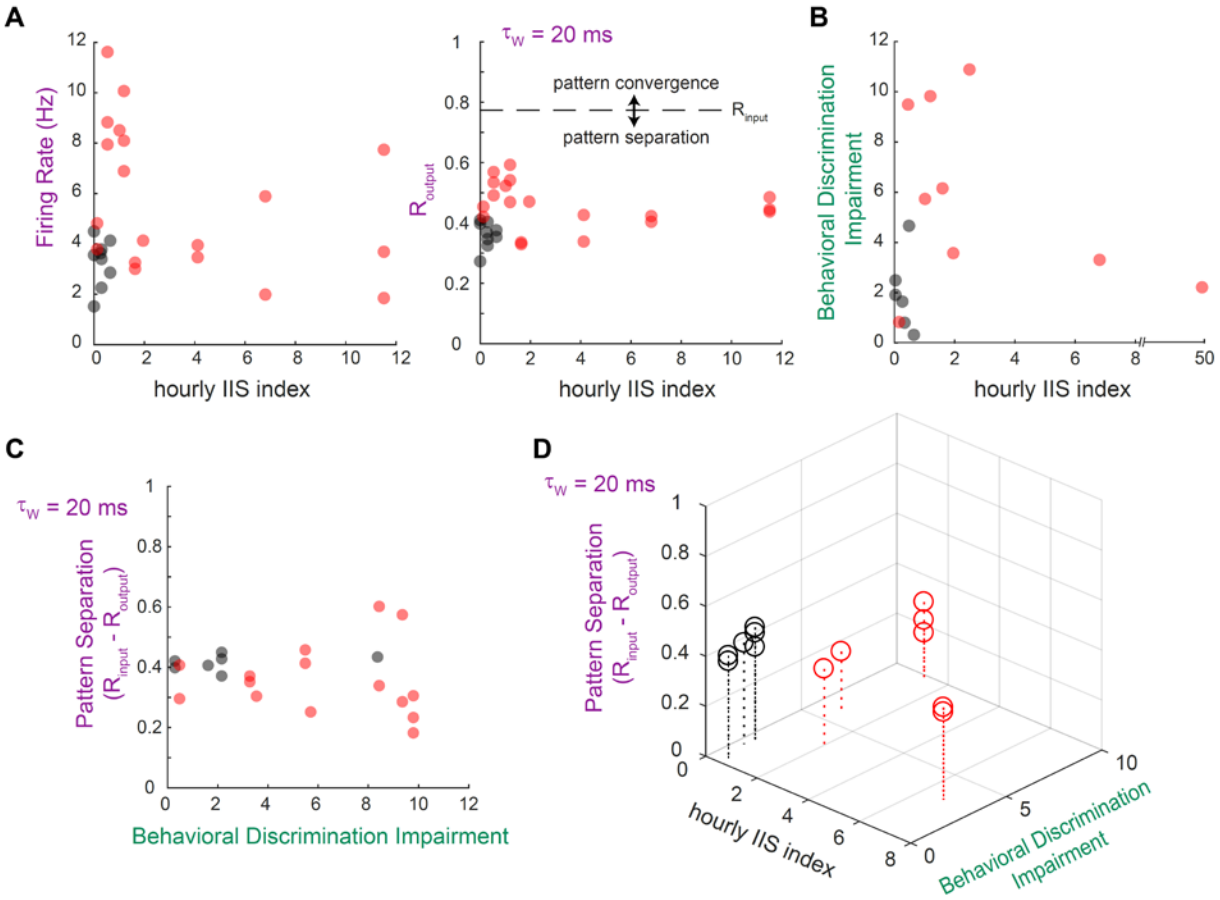


**Figure 9. EEG, behavioral and computational measures provide complementary insights about epileptic pathology in individual animals.**

**(A-D)** Scatter plots relating the electrographic measure of IISs developed in Figure 2 (black axis labels), measures from patch-clamp recordings of individual GCs from the same animals (purple axis labels) and a summary score of behavioral discrimination impairment described in Figure 3C (green axis labels). Not all three types of records are available for every animal, which leads to differences in the samples shown in each panel.

**(A)** Data points correspond to individual GCs from animals in which both IISs and patch-clamp data were recorded. Each animal has a unique average hourly IIS index value. Only a subset of GCs are outside of the Ctrl range (i.e. pathological). For example, in the mouse with the highest IIS index (~12), only one of the three recorded GCs exhibited a pathological FR (~8 Hz, left panel) and all had a similar $R_{output}$ slightly above the Ctrl range (~0.5, right panel). In contrast, some GCs with abnormally high FR (~6-12 Hz)_and $R_{output}$ (~0.5-0.6) came from animals with low IIS index (~0-2).

**(B)** Data points correspond to individual animals in which both IISs and BPS were measured. In KA animals, low IIS index can correspond to either normal or abnormal mnemonic discrimination, and despite having a high IIS index, some animals have normal discrimination.

**(C)** Data points correspond to individual GCs from animals in which both BPS and patch-clamp data were recorded. In some KA mice with large behavioral impairments and multiple recorded GCs, some GCs exhibited normal pattern separation whereas others showed pathologically low levels. The relationship is unclear, but all KA mice with large impairments had at least one pathological GC.

**(D)** Data points correspond to individual GCs from animals in which IISs, BPS and patch-clamp data were all collected. Stems show which GCs were recorded from each animal. The lower right corner would correspond to the highest pathology in electrographic, behavioral and computational categories. Despite any heterogeneity or apparent ambiguity when only one or two of these measures are considered (above), when all three measures are available for each animal, the KA group is very clearly separable from the Ctrl group.

## Discussion

We provide the first experimental evidence that TLE is characterized by both mnemonic discrimination impairments and neuronal pattern separation deficits, associated with pathological spiking behavior in a subset of GCs.

***Cognitive and computational deficits in TLE.*** Our findings are consistent with the few previous studies that focused on similar questions. First, our data in human patients confirm the findings of Reyes et al. (2018) that TLE leads to mnemonic discrimination impairments. However, they used a different behavioral paradigm: a short-term memory object-location discrimination task akin to the task we used for mice. Although animal studies suggest that DG is necessary for such spatial mnemonic discrimination (Hunsaker and Kesner, 2013; Bui et al., 2018), it remains unclear whether this is the case in humans. In contrast, we used a non-spatial memory discrimination task that is known to be DG-dependent in humans (Baker et al., 2016; Stark et al., 2019), allowing us to conclude that impairments in TLE patients are likely due to DG alterations.

Our behavioral experiment in mice (**Figure 3**) also complements a previous study (Bui et al., 2018) by testing short-term (minutes) rather than long-term (24h) object-location memory and by testing multiple, parameterized levels of mnemonic interference, as recommended for rigorous testing of mnemonic discrimination (Hunsaker and Kesner, 2013; Liu et al., 2016). As in humans, the BPS task we used in mice is likely dependent on DG activity (Bui et al., 2018).

Taken together, our results and those studies suggest that mnemonic discrimination deficits observed in TLE are shared between humans and mice, occur for different types of memory and modalities, and point to DG malfunctions.

Indeed, DG normally functions as a pattern separator (Madar et al., 2019a) which is hypothesized to support mnemonic discrimination. However, only one modelling study has so far investigated the impact of TLE-related DG pathologies on neural pattern separation (Yim et al., 2014). This model suggested that mossy fiber sprouting and increased synaptic transmission from the perforant path to GCs, both hallmarks of TLE, can theoretically lead to a breakdown of pattern separation. Our results experimentally confirm that TLE leads to a deficit in neural pattern separation (**Figure 4**). However, the deficit we observed is not as large, possibly because the model 1) considered synaptic transmission as deterministic rather than probabilistic and plastic, 2) assessed a different form of pattern separation (patterns were defined as population ensembles of very short spiketrains, thus focusing on a population code whereas we investigated temporal codes) and 3) considered more severe degrees of epilepsy than was perhaps the case for our mice.

Note that by using several similarity metrics, timescales and input statistical structures, and thus exploring various potential neural codes, we also discovered that other normal DG computations performed through rate and burstiness codes are perturbed in TLE (**Figure 5, 8**).

***The role of sparsity in neuronal pattern separation and DG gating***. We found that GCs from epileptic mice exhibit pathological spiking consistent with a breach of the DG gatekeeper function (**Figure 6**) that leads to decreased neuronal pattern separation (**Figure 8A**). As noted by others, the gating and pattern separation functions of DG may be related (Dengler and Coulter, 2016) because the filtering of incoming cortical activity into a sparser output can be a simple

mechanism underlying a form of pattern separation based on a pure population code (O'Reilly and McClelland, 1994; Severa et al., 2016; Dieni et al., 2016; Cayco-Gajic and Silver, 2019). Our results suggest that maintaining a sparse output also supports pattern separation of spiketrains in the time domain, at the level of single DGs.

Rare investigations of the spiking output of single GCs in epileptic tissue have reported that single stimulation of the perforant path sometimes leads GCs to fire bursts of spikes (Lynch et al., 2000; Kobayashi and Buckmaster, 2003). We expand on this by showing that bursts also emerge in response to complex, naturalistic stimulation patterns (**Figures 6 and 7**). It is important to note that occasional bursting is observed in normal GCs in vivo (Pernía-Andrade and Jonas, 2014), but this is very unusual in slices (Mongiat et al., 2009; Ewell and Jones, 2010; Zhang et al., 2012; Dieni et al., 2016). In our experiments, bursting GCs therefore demonstrate a breach of the dentate gate. Because bursts are known to be more efficient at driving spiking in CA3 pyramidal neurons (Henze et al., 2002), a single GC firing bursts will have a higher probability of making downstream CA3 pyramidal cells fire. This could have deleterious effects on memory encoding and promote seizures, as more active CA3 neurons would 1) increase the chance of overlap between memory representations and 2) overexcite a recurrent excitatory circuit, a mechanism of seizure generation. Thus, our findings are consistent with the idea that pathological firing or bursting of even a subset of GCs could simultaneously contribute to deficits in mnemonic discrimination and epileptiform activity in TLE.

Our study also provides new insight on the mechanisms underlying GCs increased ability to burst by testing the influence of the excitatory drive (**Figure 7B**). The main source of excitation to GCs, the perforant path, is sometimes assumed to be augmented in TLE (Yim et al., 2014) given evidence of increased release probability at the lateral perforant path synapse

(Scimemi et al., 2006). Our results do not directly contradict this, but we did not find a difference in the average synaptic current evoked in GCs by Poisson input spiketrains applied to the perforant path (**Figure 7B3**). More work is required to carefully test potential TLE-related changes in the coupling between perforant path and GCs, as well as EPSC kinetics and short-term dynamics (Madar et al., 2019a), but it is clear that the size of excitatory drive alone is not a good predictor of bursting propensity in GCs (**Figure 7B3-4**). We also previously showed that partial blockade of inhibition can produce GC bursting and pattern separation deficits (Madar et al., 2019b). Thus, in accordance with past research (Kobayashi and Buckmaster, 2003), we conclude that the strong decrease in synaptic inhibition characteristic of TLE (Dengler and Coulter, 2016; Dengler et al., 2017) is likely the main driver of pathological bursting.

Perhaps the most intriguing insight we bring on the failure of the DG as a gate and pattern separator in TLE is that this failure occurs only in a subset of GCs, upon a background of apparently normal GCs in the same the epileptic network. This finding invites many more questions: In the epileptic DG, is there a spectrum of spiking patterns among GCs going from normal to pathological, or are there two discrete types? What is the ratio of normal to pathological GCs? Does this ratio evolve during epileptogenesis? What makes individual GCs become pathological? Is that due to differences in intrinsic properties or networking? As explained above, our results suggest deficits in inhibition, but other anatomical or biophysical changes could be in play. For example, in individual mice with TLE, some GCs display pathological hilar basal dendrites that have been associated with increased intrinsic excitability that might allow them to fire bursts more easily (Kelly and Beck, 2017). It is also possible that there exist heterogeneity in GC mossy fiber sprouting, with some GCs receiving recurrent excitatory connections and some not. Some of these differences could be related to different

875 birthdates of adult-born GCs relative to an epileptogenic brain insult, resulting in only a subset of
876 GCs integrating abnormally into the DG network (Kron et al., 2010). Alternatively, pathological
877 GCs could develop from a more susceptible and active subclass of mature GCs (Erwin et al.,
878 2019). In any case, the discovery that the GC population in the epileptic DG is not homogeneous
879 in terms of spiking patterns is a crucial step towards developing new treatments that would
880 specifically target pathological neurons to avoid deleterious side-effects (Bielefeld et al., 2014).

881 ***The link between mnemonic discrimination, pattern separation and TLE.*** For thirty
882 years the DG has been hypothesized to support mnemonic discrimination by performing
883 neuronal pattern separation (Treves et al., 2008), but no experiment has yet directly connected
884 DG input-output computations with memory. Important reports have shown that 1) abnormal
885 neurotransmission in the DG can lead to overlapping spatial representations in CA3 as well as
886 impairments in context discrimination learning (McHugh et al., 2007) and 2) that overlapping
887 engrams in DG are a cause of confusion between the associated memories (Ramirez et al., 2013).
888 However, those reports did not investigate whether pattern separation was performed in the DG
889 per se, as opposed to upstream areas. Here, we confirm our previous work showing that the DG
890 itself performs temporal pattern separation (Madar et al., 2019a, b) and we show that, on
891 average, a deficit in pattern separation is associated with a deficit in mnemonic discrimination. A
892 full demonstration of the causal link will require measuring and manipulating DG computations
893 in vivo during episodic memory tasks, but our study is a preliminary step toward understanding
894 how DG circuit-level computations relate to a high-level cognitive function and how these
895 processes fail in TLE. A mechanistic understanding of this relation may lead to new early
896 diagnosis tools (e.g. cognitive tests like in Figure 1) as well as therapies alleviating memory
897 disorders in TLE. For example, our finding that a subset of GCs with pattern separation deficits

898 can develop without EEG hallmarks of epilepsy (**Figure 9A**) suggests a mechanism for memory
899 impairments that often occur in early stages of human epileptogenesis (Jones et al., 2007; Witt
900 and Helmstaedter, 2015) and the coexistence of pathological and normal neurons could explain
901 memory impairments without hippocampal sclerosis (Rayner et al., 2019).

902 ## References
903
904 Alexander A, Maroso M, Soltesz I (2016) Organization and control of epileptic circuits in temporal lobe epilepsy.
905 Progress in brain research 226:127-154.
906 Artinian J, Peret A, Marti G, Epsztein J, Crepel V (2011) Synaptic kainate receptors in interplay with INaP shift the
907 sparse firing of dentate granule cells to a sustained rhythmic mode in temporal lobe epilepsy. The Journal
908 of neuroscience : the official journal of the Society for Neuroscience 31:10811-10818.
909 Baker S, Vieweg P, Gao F, Gilboa A, Wolbers T, Black SE, Rosenbaum RS (2016) The Human Dentate Gyrus
910 Plays a Necessary Role in Discriminating New Memories. Current biology : CB.
911 Behr J, Lyson KJ, Mody I (1998) Enhanced propagation of epileptiform activity through the kindled dentate gyrus.
912 Journal of neurophysiology 79:1726-1732.
913 Bennett IJ, Stark CE (2016) Mnemonic discrimination relates to perforant path integrity: An ultra-high resolution
914 diffusion tensor imaging study. Neurobiology of learning and memory 129:107-112.
915 Berron D, Schutze H, Maass A, Cardenas-Blanco A, Kuijf HJ, Kumaran D, Duzel E (2016) Strong Evidence for
916 Pattern Separation in Human Dentate Gyrus. The Journal of neuroscience : the official journal of the
917 Society for Neuroscience 36:7569-7579.
918 Bielefeld P, van Vliet EA, Gorter JA, Lucassen PJ, Fitzsimons CP (2014) Different subsets of newborn granule
919 cells: a possible role in epileptogenesis? The European journal of neuroscience 39:1-11.
920 Bui AD, Nguyen TM, Limouse C, Kim HK, Szabo GG, Felong S, Maroso M, Soltesz I (2018) Dentate gyrus mossy
921 cells control spontaneous convulsive seizures and spatial memory. Science 359:787-790.
922 Cayco-Gajic NA, Silver RA (2019) Re-evaluating Circuit Mechanisms Underlying Pattern Separation. Neuron
923 101:584-602.
924 Chavlis S, Poirazi P (2017) Pattern separation in the hippocampus through the eyes of computational modeling.
925 Synapse (New York, NY).
926 Coras R, Pauli E, Li J, Schwarz M, Rossler K, Buchfelder M, Hamer H, Stefan H, Blumcke I (2014) Differential
927 influence of hippocampal subfields to memory formation: insights from patients with temporal lobe
928 epilepsy. Brain : a journal of neurology 137:1945-1957.
929 Coulter DA, Carlson GC (2007) Functional regulation of the dentate gyrus by GABA-mediated inhibition. 163:235-
930 812.
931 De Maesschalck R, Jouan-Rimbaud D, Massart DL (2000) The mahalanobis distance. Chemometrics and intelligent
932 laboratory systems 50:1-18.
933 Dengler CG, Coulter DA (2016) Normal and epilepsy-associated pathologic function of the dentate gyrus. Progress
934 in brain research 226:155-178.
935 Dengler CG, Yue C, Takano H, Coulter DA (2017) Massively augmented hippocampal dentate granule cell
936 activation accompanies epilepsy development. Scientific reports 7:42090.
937 Dieni CV, Panichi R, Aimone JB, Kuo CT, Wadiche JI, Overstreet-Wadiche L (2016) Low excitatory innervation
938 balances high intrinsic excitability of immature dentate neurons. Nature communications 7:11313.
939 Dillon SE, Tsivos D, Knight M, McCann B, Pennington C, Shiel AI, Conway ME, Newson MA, Kauppinen RA,
940 Coulthard EJ (2017) The impact of ageing reveals distinct roles for human dentate gyrus and CA3 in
941 pattern separation and object recognition memory. Scientific reports 7:14069.
942 Erwin SR, Sun W, Copeland M, Lindo S, Spruston N, Cembrowski MS (2019) A sparse, spatially biased subtype of
943 mature granule cell is preferentially recruited in hippocampal-associated behaviors. bioRxiv:804393.
944 Ewell LA, Jones MV (2010) Frequency-tuned distribution of inhibition in the dentate gyrus. The Journal of
945 neuroscience : the official journal of the Society for Neuroscience 30:12597-12607.
946 Groticke I, Hoffmann K, Loscher W (2008) Behavioral alterations in a mouse model of temporal lobe epilepsy
947 induced by intrahippocampal injection of kainate. Experimental neurology 213:71-83.

948 Hellier JL, Patrylo PR, Buckmaster PS, Dudek FE (1998) Recurrent spontaneous motor seizures after repeated low-
949 dose systemic treatment with kainate: assessment of a rat model of temporal lobe epilepsy. Epilepsy
950 research 31:73-84.
951 Helmstaedter C, Kurthen M, Lux S, Reuber M, Elger CE (2003) Chronic epilepsy and cognition: a longitudinal
952 study in temporal lobe epilepsy. Annals of neurology 54:425-432.
953 Henze DA, Wittner L, Buzsaki G (2002) Single granule cells reliably discharge targets in the hippocampal CA3
954 network in vivo. Nature neuroscience 5:790-795.
955 Hsu D (2007) The dentate gyrus as a filter or gate: a look back and a look ahead. Progress in brain research 163:601-
956 613.
957 Hunsaker MR, Kesner RP (2013) The operation of pattern separation and pattern completion processes associated
958 with different attributes or domains of memory. Neuroscience and biobehavioral reviews 37:36-58.
959 Inostroza M, Brotons-Mas JR, Laurent F, Cid E, de la Prida LM (2013) Specific impairment of "what-where-when"
960 episodic-like memory in experimental models of temporal lobe epilepsy. Journal of Neuroscience
961 33:17749-17762.
962 Jones JE, Watson R, Sheth R, Caplan R, Koehn M, Seidenberg M, Hermann B (2007) Psychiatric comorbidity in
963 children with new onset epilepsy. Developmental medicine and child neurology 49:493-497.
964 Kelly T, Beck H (2017) Functional properties of granule cells with hilar basal dendrites in the epileptic dentate
965 gyrus. Epilepsia 58:160-171.
966 Kesner RP, Rolls ET (2015) A computational theory of hippocampal function, and tests of the theory: new
967 developments. Neuroscience and biobehavioral reviews 48:92-147.
968 Kesner RP, Kirk RA, Yu Z, Polansky C, Musso ND (2016) Dentate gyrus supports slope recognition memory,
969 shades of grey-context pattern separation and recognition memory, and CA3 supports pattern completion
970 for object memory. Neurobiology of learning and memory 129:29-37.
971 Knierim JJ, Neunuebel JP (2016) Tracking the flow of hippocampal computation: Pattern separation, pattern
972 completion, and attractor dynamics. Neurobiology of learning and memory 129:38-49.
973 Kobayashi M, Buckmaster PS (2003) Reduced inhibition of dentate granule cells in a model of temporal lobe
974 epilepsy. The Journal of neuroscience : the official journal of the Society for Neuroscience 23:2440-2452.
975 Kron MM, Zhang H, Parent JM (2010) The developmental stage of dentate granule cells dictates their contribution
976 to seizure-induced plasticity. The Journal of neuroscience : the official journal of the Society for
977 Neuroscience 30:2051-2059.
978 Krook-Magnuson E, Armstrong C, Bui A, Lew S, Oijala M, Soltesz I (2015) In vivo evaluation of the dentate gate
979 theory in epilepsy. The Journal of physiology 593:2379-2388.
980 Le Duigou C, Simonnet J, Telenczuk MT, Fricker D, Miles R (2014) Recurrent synapses and circuits in the CA3
981 region of the hippocampus: an associative network. Frontiers in cellular neuroscience 7:262.
982 Lee CT, Kao MH, Hou WH, Wei YT, Chen CL, Lien CC (2016) Causal Evidence for the Role of Specific
983 GABAergic Interneuron Types in Entorhinal Recruitment of Dentate Granule Cells. Scientific reports
984 6:36885.
985 Lenck-Santini PP, Scott RC (2015) Mechanisms Responsible for Cognitive Impairment in Epilepsy. Cold Spring
986 Harbor perspectives in medicine 5.
987 Levesque M, Avoli M (2013) The kainic acid model of temporal lobe epilepsy. Neuroscience and biobehavioral
988 reviews 37:2887-2899.
989 Levesque M, Avoli M, Bernard C (2016) Animal models of temporal lobe epilepsy following systemic
990 chemoconvulsant administration. Journal of neuroscience methods 260:45-52.
991 Lilliefors HW (1967) On the Kolmogorov-Smirnov test for normality with mean and variance unknown. Journal of
992 the American statistical Association 62:399-402.
993 Liu KY, Gould RL, Coulson MC, Ward EV, Howard RJ (2016) Tests of pattern separation and pattern completion
994 in humans-A systematic review. Hippocampus 26:705-717.
995 Lu Y, Zhong C, Wang L, Wei P, He W, Huang K, Zhang Y, Zhan Y, Feng G, Wang L (2016) Optogenetic
996 dissection of ictal propagation in the hippocampal–entorhinal cortex structures. Nature communications
997 7:10962.
998 Lynch M, Sayin U, Golarai G, Sutula T (2000) NMDA receptor-dependent plasticity of granule cell spiking in the
999 dentate gyrus of normal and epileptic rats. Journal of neurophysiology 84:2868-2879.
1000 Madar AD, Ewell LA, Jones MV (2019a) Pattern separation of spiketrains in hippocampal neurons. Scientific
1001 reports 9:5282.
1002 Madar AD, Ewell LA, Jones MV (2019b) Temporal pattern separation in hippocampal neurons through multiplexed
1003 neural codes. PLoS computational biology 15:e1006932.

McHugh TJ, Jones MW, Quinn JJ, Balthasar N, Coppari R, Elmquist JK, Lowell BB, Fanselow MS, Wilson MA, Tonegawa S (2007) Dentate gyrus NMDA receptors mediate rapid pattern separation in the hippocampal network. Science 317:94-99.

Mongiat LA, Esposito MS, Lombardi G, Schinder AF (2009) Reliable activation of immature neurons in the adult hippocampus. PloS one 4:e5320.

Motulsky HJ, Ransnas LA (1987) Fitting curves to data using nonlinear regression: a practical and nonmathematical review. FASEB journal : official publication of the Federation of American Societies for Experimental Biology 1:365-374.

Muller CJ, Groticke I, Bankstahl M, Loscher W (2009) Behavioral and cognitive alterations, spontaneous seizures, and neuropathology developing after a pilocarpine-induced status epilepticus in C57BL/6 mice. Experimental neurology 219:284-297.

O'Reilly RC, McClelland JL (1994) Hippocampal conjunctive encoding, storage, and recall: avoiding a trade-off. Hippocampus 4:661-682.

Ouedraogo DW, Lenck-Santini PP, Marti G, Robbe D, Crepel V, Epsztein J (2016) Abnormal UP/DOWN Membrane Potential Dynamics Coupled with the Neocortical Slow Oscillation in Dentate Granule Cells during the Latent Phase of Temporal Lobe Epilepsy. eNeuro 3.

Pardi MB, Ogando MB, Schinder AF, Marin-Burgin A (2015) Differential inhibition onto developing and mature granule cells generates high-frequency filters with variable gain. eLife 4:e08764.

Patrylo PR, Schweitzer JS, Dudek FE (1999) Abnormal responses to perforant path stimulation in the dentate gyrus of slices from rats with kainate-induced epilepsy and mossy fiber reorganization. Epilepsy research 36:31-42.

Pernía-Andrade Alejandro J, Jonas P (2014) Theta-Gamma-Modulated Synaptic Currents in Hippocampal Granule Cells In Vivo Define a Mechanism for Network Oscillations. Neuron 81:140-152.

Pfammatter JA, Bergstrom RA, Wallace EP, Maganti RK, Jones MV (2018) A predictive epilepsy index based on probabilistic classification of interictal spike waveforms. PloS one 13:e0207158.

Racine RJ (1972) Modification of seizure activity by electrical stimulation: II. Motor seizure. Electroencephalography and clinical neurophysiology 32:281-294.

Ramirez S, Liu X, Lin PA, Suh J, Pignatelli M, Redondo RL, Ryan TJ, Tonegawa S (2013) Creating a false memory in the hippocampus. Science 341:387-391.

Rayner G, Tailby C, Jackson G, Wilson S (2019) Looking beyond lesions for causes of neuropsychological impairment in epilepsy. Neurology 92:e680-e689.

Reyes A, Holden HM, Chang YA, Uttarwar VS, Sheppard DP, DeFord NE, DeJesus SY, Kansal L, Gilbert PE, McDonald CR (2018) Impaired spatial pattern separation performance in temporal lobe epilepsy is associated with visuospatial memory deficits and hippocampal volume loss. Neuropsychologia 111:209-215.

Rolls ET (2010) A computational theory of episodic memory formation in the hippocampus. Behavioural brain research 215:180-196.

Santoro A (2013) Reassessing pattern separation in the dentate gyrus. Frontiers in behavioral neuroscience 7:96.

Scimemi A, Schorge S, Kullmann DM, Walker MC (2006) Epileptogenesis is associated with enhanced glutamatergic transmission in the perforant path. Journal of neurophysiology 95:1213-1220.

Severa W, Parekh O, James CD, Aimone JB (2016) A Combinatorial Model for Dentate Gyrus Sparse Coding. Neural computation:1-24.

Sharma S, Puttachary S, Thippeswamy A, Kanthasamy AG, Thippeswamy T (2018) Status epilepticus: Behavioral and electroencephalography Seizure Correlates in Kainate experimental Models. Frontiers in neurology 9:7.

Simon P, Dupuis R, Costentin J (1994) Thigmotaxis as an index of anxiety in mice. Influence of dopaminergic transmissions. Behavioural brain research 61:59-64.

Sloviter RS (1983) "Epileptic" brain damage in rats induced by sustained electrical stimulation of the perforant path. I. Acute electrophysiological and light microscopic studies. Brain research bulletin 10:675-697.

Stark SM, Kirwan CB, Stark CEL (2019) Mnemonic Similarity Task: A Tool for Assessing Hippocampal Integrity. Trends in cognitive sciences.

Stark SM, Yassa MA, Lacy JW, Stark CE (2013) A task to assess behavioral pattern separation (BPS) in humans: Data from healthy aging and mild cognitive impairment. Neuropsychologia 51:2442-2449.

Tellez-Zenteno JF, Hernandez-Ronquillo L (2012) A review of the epidemiology of temporal lobe epilepsy. Epilepsy research and treatment 2012:630853.

Toyoda I, Bower MR, Leyva F, Buckmaster PS (2013) Early activation of ventral hippocampus and subiculum during spontaneous seizures in a rat model of temporal lobe epilepsy. The Journal of neuroscience : the official journal of the Society for Neuroscience 33:11100-11115.

Treves A, Tashiro A, Witter MP, Moser EI (2008) What is the mammalian dentate gyrus good for? Neuroscience 154:1155-1172.

van Hagen BT, van Goethem NP, Lagatta DC, Prickaerts J (2015) The object pattern separation (OPS) task: a behavioral paradigm derived from the object recognition task. Behavioural brain research 285:44-52.

Wallace E, Kim DY, Kim KM, Chen S, Blair Braden B, Williams J, Jasso K, Garcia A, Rho JM, Bimonte-Nelson H, Maganti R (2015) Differential effects of duration of sleep fragmentation on spatial learning and synaptic plasticity in pubertal mice. Brain research 1615:116-128.

Witt JA, Helmstaedter C (2015) Cognition in the early stages of adult epilepsy. Seizure 26:65-68.

Yassa MA, Mattfeld AT, Stark SM, Stark CE (2011) Age-related memory deficits linked to circuit-specific disruptions in the hippocampus. Proceedings of the National Academy of Sciences of the United States of America 108:8873-8878.

Yi F, Catudio-Garrett E, Gabriel R, Wilhelm M, Erdelyi F, Szabo G, Deisseroth K, Lawrence J (2015) Hippocampal "cholinergic interneurons" visualized with the choline acetyltransferase promoter: anatomical distribution, intrinsic membrane properties, neurochemical characteristics, and capacity for cholinergic modulation. Frontiers in synaptic neuroscience 7:4.

Yim MY, Hanuschkin A, Wolfart J (2014) Intrinsic rescaling of granule cells restores pattern separation ability of a dentate gyrus network model during epileptic hyperexcitability. Hippocampus.

Zhang W, Huguenard JR, Buckmaster PS (2012) Increased excitatory synaptic input to granule cells from hilar and CA3 regions in a rat model of temporal lobe epilepsy. The Journal of neuroscience : the official journal of the Society for Neuroscience 32:1183-1196.

Zhao F, Kang H, You L, Rastogi P, Venkatesh D, Chandra M (2014) Neuropsychological deficits in temporal lobe epilepsy: A comprehensive review. Annals of Indian Academy of Neurology 17:374-382.